DEVELOPMENT OF RGO/PANI/PVA-BASED ELECTROSPUN NANOCOMPOSITES

by

SAJJAD GHOBADI

Submitted to the Graduate School of Engineering and Natural Sciences

in partial fulfillment of

the requirements for the degree of

Master of Science

Sabancı University

July 2015

Development of rGO/PANI/PVA-Based Electrospun Nanocomposites

APPROVED BY:

Assoc. Prof. Dr.Selmiye Alkan Gürsel	(Thesis Supervisor)	.....
Asst. Prof. Dr. Fevzi Çakmak Cebebi	(Thesis Co-advisor)	.....
Assoc. Prof. Dr. Melih Papila	(Thesis Co-advisor)	.....
Asst. Prof. Dr. Elif Özden Yenigün		.....
Assoc. Prof. Dr. Güllü Kızıltaş Şendur		.....

DATE OF APPROVAL: 28/07/2015

Development of rGO/PANI/PVA-Based Electrospun Nanocomposites

Sajjad Ghobadi

Materials Science and Engineering, MSc Thesis, 2015

Thesis Supervisor: Assoc. Prof. Dr. Selmiye Alkan Gürsel

Thesis Co-advisors: Assist. Prof. Dr. Fevzi Çakmak Cebeci, Assoc. Prof. Dr. Melih Papila

Keywords: Graphene, Electrospinning, Nanocomposite, Colloidal Suspension

Abstract

In this project, with the scope electromechanically responsive nanocomposite applications, fibrous nanocomposites with various filler compositions based on poly(vinyl alcohol) (PVA) as the polymer matrix, reduced graphene oxide (rGO), and polyaniline (PANI) as conductive reinforcing filler components were successfully prepared via electrospinning and their relative properties were systematically investigated.

Prior to electrospinning suspension preparation, graphene oxide (GO) was prepared from natural graphite flakes through an improved method based on Hummer's Modified conventional method. Subsequently, high temperature thermal treatment on the as-prepared GO resulted in formation of thermally reduced GO. Additionally, PANI nanofibers were synthesized via chemical oxidation polymerization starting from aniline monomer.

After optimization of PVA concentration in electrospinning media, two main nanofiber preparation and characterization steps were designed and conducted according to the following procedures.

Firstly, incorporation of reduced graphene oxide of certain amounts in the electrospinning media was performed by means of co-solvent assisted suspension preparation method proposed by our group followed by electrospinning of respective solutions. Rheological behavior of electrospinning suspensions in addition to morphological, mechanical and thermal properties of their respective as-spin mats was investigated.

Secondly, PANI as the electroactive polymer was introduced to the electrospinning suspension recipe optimized during the previous step. In order to improve electrical conductivity of mentioned tri-component PVA/rGO/ PANI as-spun mats, two different post-spinning treatment approaches were performed.

The first modification applied included cross-linking of electrospun thin mats using the glutaraldehyde solution, followed by doping of emeraldine base PANI inside the structure, during which, further transformation of PANI state to conductive emeraldine salt was achieved and confirmed by Fourier-Transformed IR spectroscopy (FT-IR).

The second modification approach used was thermal treatment through a neutral gas-condition annealing process. The main goal to pursue this method was to both partially eliminate the insulating PVA matrix as well as thermal doping of PANI.

While the as-spun showed no response to applied voltages and performed as insulating layers, the post-treated samples showed relatively improved electrical properties and the highest electrical conductivity was peaked at over $19 \mu S.cm^{-1}$.

RGO/PANI/PVA Esaslı Nanokompozitlerin Elektrodokuma ile Üretilmesi ve Geliştirilmesi

Sajjad Ghobadi

Malzeme Bilimi ve Mühendisliği, MSc Tezi, 2015

Tez Danışmanı: Doç. Dr. Selmiye Alkan Gürsel

Ortak Tez Danışmanı: Yar. Doç. Dr. Fevzi Çakmak Cebeci, Doç. Dr.Melih Papila

Anahtar Kelimeler: Grafen, Elektrodokuma, Nanokompozit, Kolloid Süspansiyon

Özet

Bu tez kapsamında, lifli yapıdaki nanokompozitlerin; poli(vinil alkol) (PVA)'ün taşıyıcı polimer matrisi olarak, indirgenmiş grafen oksit (GO) ve polianilin (PANI)'nin ise iletken dolgu bileşenleri olarak kullanılarak elektrodokuma yöntemiyle hazırlanması ve özelliklerinin sistematik olarak incelenmesi sayesinde elektromekanik olarak cevap verebilen nanokompozit uygulamalarında kullanılabilecek nanokompozitlerin geliştirilmesi başarıyla gerçekleştirilmiştir.

Elektrodokuma işleminden önce, grafen oksit grafit kullanılarak modifiye Hummer's yöntemiyle sentezlenmiştir. Ardından gerçekleştirilen termal işlem ile termal olaraak indirgenmiş GO üretilmiştir. PANI nanofiberleri ise kimyasal polimerleşme ile anilinden başlanarak üretilmiştir.

Öncelikle elektrodokuma ortamındaki PVA derişimi optimize edilmiş, ardından da nanofiberlerin hazırlanması ve karakterizasyonları gerçekleştirilmiştir. Bu amaç için, değişen miktarlarda grafen oksitin yapıya entegrasyonu için tarafımızca geliştirmiş olan ko-çözücü varlığında hazırlanan süspansiyon yöntemi başarıyla uygulanmış ve elektrodokuma işlemi geliştirilmiştir. Elektrodokuma öncesinde, hazırlanan süspansiyonların reolojik özellikleri detaylı olarak incelenmiştir. Elektrodokuma sonrasında elde edilen nanokompozitlerin ise, morfolojik, mekanik ve ısıl özellikleri detaylı olarak karakterize edilmiştir.

İlk olarak uygulanan modifikasyon işlemi, elde edilen nanokompozitlerin glutaraladehit çözeltisi kullanılarak çapraz bağlanması ve ardından da PANI'nin (emeraldin) katkılandırılması olmuştur. Böylelikle yapı içindeki PANI'nin iletkenlik kazanması sağlanmış ve elde edilen yapı FTIR spektroskopisi ile karakterize edilmiştir.

İkinci modifikasyon işlemi ise nötr bir gaz ortamında tavlama şeklinde gerçekleştirilen termal işlemdir. Bu işlemin amacı ise, yapıda bulunan iletken olmayan PVA'yı kısmen yapıdan uzaklaştırmak ve PANI'nin ısıl katkılandırmasını gerçekleştirmektir.

Elektrodokuma ile üretilmiş nanokompozitlerin uygulanan voltajlara karşı tepki göstermemesine ve iletkenliklerin oldukça düşük olmasına karşın, uygulanan modifikasyonlar (çapraz bağlama, ısıl işlem ve asit ile katkılandırma) sayesinde iletkenlik kazandıkları görülmüş ve 19$\mu S.cm^{-1}$ civarında iletkenlikler elde edilebilmiştir.

Acknowledgement

I would like to express my deep gratitude to all the people who have never hesitated to support me by any means possible to fulfill this goal.

I would like to gracefully thank my advisor, Prof. Dr. Selmiye Alkan Gürsel, for not only her scientific and academic support during this period but also that she always cared about my personal life as an international student. I cannot thoroughly express my feeling of appreciation about the opportunity of working in a friendly, hardworking, extremely collaborative team provided with me by her.

I want to also mention my sincere appreciation to my co-advisors, Prof. Dr. Fevzi Çakmak Cebeci and Prof. Dr. Melih Papila, whom during this period have never stopped devoting their time and resources to my work and the constructive discussions with them have always been of tremendous help to pave my way through success not only in this work but also in all matters of academic life.

I wanted to also thank my thesis dissertation defense jury that have honored me by accepting to be members of my defense jury and have reviewed this dissertation with meticulous consideration.

My best regards and many thanks goes to my fellow graduate students of materials science and engineering program who have always kept the work atmosphere as friendly and cooperative as possible and taught me how to be a better person along with being a respectable academician. In that matter, my best wishes goes to my co-workers in polymer synthesis and characterization lab specially Jamal Seyed Monfared Zanjani, Shayan Mehrayeen, Omid Akhlaghi Baghoojari, Zahra Gohari Bajestani, Kaan Bilge, and all those whom their name wasn't mentioned here.

Last but not least, I wanted to salute the support of my lovely family who has always supported me by any means necessary and proved me that "we can be so far in distance yet so close in each other's hearts".

Sajjad Ghobadi

To my beloved uncle, Mohammad Ali, who sacrificed his young life defending my country.

Table of Contents

List of Figures

List of Tables

1. Introduction

1.1. Graphene, Synthesis, Properties and Applications

Graphene as a 2D material with single-atom layered structure of sp^2 carbon atoms has drawn significant attention among research groups around the world [1]. Superior mechanical, thermal and electrical properties along with extremely high specific surface area are defining characteristics of material. At desirable conditions, graphene with Young modulus value of over 1TPa, thermal conductivity of 5000 $Wm^{-1}K^{-1}$, specific surface area of 2630 m^2g^{-1}, and 20 $m^2V^{-1}s^{-1}$ value for its relative charge carrier mobility can be obtained[2, 3].

High level properties of graphene were shown to result in to have a reinforcing role via its incorporation in synthetic materials for different purposes, such as sensor applications [4,5], electronics[6], fuel cell membranes [7], and mechanical reinforcement applications[8, 9]. Regarding the mentioned potential applications of graphene, particularly 2D-filler performance of the material and its derivatives in polymer based nanocomposites has been proved to be promising [10, 11].

Peng and co-workers[12] prepared palladium-tailored graphene template surfaces on silicon wafer substrate. Within that work it was shown that such a device was successfully used for hydrogen sensing purposes. Magnetic sensing ability was also added by gold nanoparticle modification of Graphene layers.

Shakir's research team [13] prepared high capacitance-high energy density graphene/multi-walled carbon nanotubes (MWCNT) flexible super capacitors via layer-by-layer (LBL) self-assembly method. It was shown that through this approach carbon nanotubes acted as layer exfoliation improving particles, further enhancing capacitance performance of prepared devices. As-prepared super capacitors showed 400 f/g specific capacitance and energy density of 50-200 Wh/kg. However, a dramatic specific capacitance decrease was observed at over 500 operation cycles.

As a novel method for preparation of catalyst layers, nitrogen-doped graphene catalysts have been prepared by Qiao's group for oxygen reduction process catalysis in fuel cell applications[14]. By addition of graphene oxide (GO) dispersion into a silica sphere suspension, the template assisted GO structure was formed and followed by multiple aggressive acid treatment and pyrolysis after which the GO catalyst layer was obtained.

Desirable catalytic activity of as-prepared catalysts was confirmed via cyclic voltammetry and linear sweep voltammetry analyses further acknowledging application of graphene-based catalyst templates for fuel cell operating systems.

Khanna and co-workers used graphene few layers as mechanically reinforcing components in polyurethane films [15]. The molding solution was prepared via solution mixing of graphene dispersion and PU solution in a one-pot process. Some of the prepared specimens were post heated for comparison. The results of universal testing machine (UTM) analysis of the prepared samples showed 30% increase in graphene-containing specimens' Tensile strength in comparison with those of pristine PU ones. However a decrease in strain at breakage point was observed which was due to brittleness of graphene structure. Further improvement in composite's mechanical properties was achieved by post-heat- treatment resulting in a further 20% increase in specimens' tensile strength with respect to the recorded values for pristine, untreated PU samples.

1.2. Graphene Preparation Methods

The basis for graphene preparation is to increase the inter-layer spacing of graphite layers to the extent of which they can be easily separated and dispersed in different media. Since the discovery of graphite structure, there has been a huge interest into preparation of exfoliated graphite, known as graphene, among the researchers around the world. Among the vast variety of synthesis methods such as chemical vapor deposition (CVD) [16], Solvent-assisted exfoliation[17], and chemically oxidative oxidation[1], the last one was chosen to be used in this study. The ease of preparation, and the ability to have control on final products chemical functionalities were among the main reasons for choosing that specific approach for this study.

Chongwu et al. [16] have comprehensively reviewed graphene structures prepared via chemical vapor deposition through different processes. The effectiveness of each process based on the changes in used substrate (such as Ni foam, Si-SiO_2 wafers, etc.) and the treatments conducted on the products were also investigated with respect final products' attributes like mechanical, thermal and electrical properties. Growth of huge-grain graphene monolayers with over 100μm diameters on Si-SiO_2 (known as silicon wafer) substrate was reported to be effectively used for field effect transistors.

Khan and coworkers [18] presented three different approaches for preparation of few-layer graphene nanosheets based on solvent assisted exfoliation of graphite layered structure. The ultimately desired few-layer thickness graphene were obtained via initial ultrasonic dispersion of graphite into N-methyl-2-pyrrolidone (NMP) solvent followed by numerous bath sonication bath-centrifugation coupled steps for over 200 hours, of total sonication period, on the supernatant fluid of each step's centrifugation product. The final extremely high concentration (63 wt%) graphene dispersion reached unlimited stability due to formation of gel-like orientation of graphene layers. Raman spectroscopy assisted by TEM imaging confirmed perfect exfoliation graphite structure, thus formation of few-layer graphene. Further statistical investigation on sedimentation amount versus time for samples prepared with different sonication periods resulted in proposing a formulation for prediction of sedimentation fraction with respect to sample rest time. Control samples' records showed consistency between estimations calculated by the model and experimentally recorded values.

The chemical oxidation of natural graphite flakes resulting functionalization and layer-exfoliation of graphene layers was conducted by Marcano's research group[1]. During that study a comparison between products Hummer's, Modified Hummer's[19], and an improved method based on the Modified Hummer's method was reported. As-prepared GO sheets were then chemically reduced followed by thermal annealing at 900°C to eliminate the functional groups. It was shown that via the improved method, extremely poisonous nitrogen oxide gases (NO_x) production during the oxidation process as the side product of the other two methods was eliminated. Additionally, higher level of oxidation (69%) in comparison with Hummer's methods was achieved. The finally obtained rGO nanolayers produced by improved method possessed superior electrical conductivity values being 2 times fold higher than conventional synthesis method products.

Botas et al. [20] comprehensively studied effect of temperature on reduction graphene oxide (GO) through the thermal exfoliation process producing rGO structures. Noticeable changes in functionality, functional group layer-coverage area, and layer wrinkling was shown with respect to annealing temperature. The Nucleic Magnetic Resonance (NMR) spectra of as-prepared rGO samples revealed that the major thermal reduction of GO layers happen at 250-350°C where complete functional group removal takes place at 1000°C. However, the wrinkled layers was still present after the

mentioned high-temperature treatment. Complete layer-straightening process was achieved at extremely higher annealing temperature of 2400°C resulting in production of unwrinkled graphene layers with no oxygen-containing functional groups present.

1.3. Electrically Conductive Polymers

There is a specific type of polymers which have the potential ability to conduct electricity in their structure. They are also known as intrinsically conductive polymers. As they are organic compounds, due to variations possible in their synthesis process, they can reach metallic electrical properties or act as semiconductors with lower electrical conductivities. As a result they are also called synthetic metals.

The most important advantage of using such polymers is that as they are organic compounds they can be processed through preparation of a homogeneous dispersion of them in different types of solvents. However, they are not thermoplastic and cannot be formed by applying heat.

The mechanism of electrical conductivity in the mentioned polymers is based on presence of conjugate π-π bonds resulting in generation of delocalized electrons of sp^2 bonds in the polymer structure. Thus, the charge carrying process is completed by the mentioned delocalized electrons along the polymer backbone. The conjugate bonds in conductive polymers mainly form within the aromatic cycle parts of polymer backbone such as polypyrrole , polyaniline (PANI), and polythiophene [21], while there are other conductive polymers which their electrical conductivity roots through their conjugate carbon-carbon double bonds in their structure. Polyacetylene is an example of these type of conductive polymers.

Among the conductive polymers with aromatic cycles present in their backbone, Polyaniline is a well-known conductive polymer which has shown to perform in different applications promisingly. The chemical structure of PANI consists of aromatic cycles inter-connected through nitrogen atoms via conjugate bonds (fig. 1).

There are three reported states for PANI among which only one state possess electrical conductivity. They are named as pernigraniline, leucoemeraldine, and emeraldine salt states, respectively. As it is shown in the fig.1 the fraction ratio of m/n in the prepared PANI determined through the polymerization process, is the key factor in determination of PANI's state as well as its relative electrical properties. The pernigraniline and

leucoemeraline states of the polymer are fully oxidized and fully reduced states of PANI, respectively. Thus such materials possess no electrical conductivity. The only conductive state of PANI is the emeraldine state which can either be in the partially oxidized state which is called emeraldine salt or by reduction transform into the partially reduced state, known as emeraldine base state (Fig.1). The oxidation and reduction of PANI is known as doping and de-doping processes, respectively.

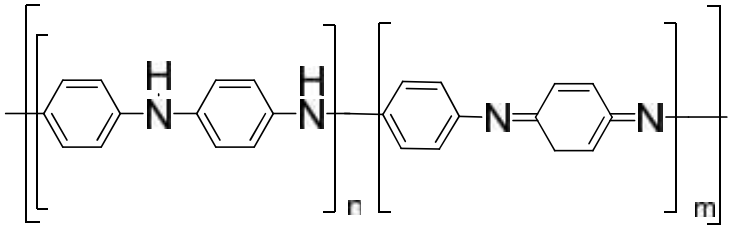

Figure 1 The Chemical Structure of Polyaniline.

As shown in fig.1, the m and n values are defining factors for PANI's state where always m + n=1. Leucoemeraldine state will be obtained when m=0 and n=1, and similar to that, pernigraniline and emeraldine salts will be achieved in the material when the conditions are (n=0, m=1), and (n=m=0.5), respectively.

Focusing on emeraldine state of PANI, the natural behavior of the polymer would change upon its condition. Doped emeraldine salt (ES) PANI which is at its oxidized state possess high ionic conductivity and has dark green color where the de-doped (reduced) state, known as emeraldine base [8], has a dark purple color. The emeraldine salt PANI can only be dispersed in highly acidic solutions, where most of polar organic solvents, such as dimethylformamide (DMF) or dimethylsulfoxide (DMSO) can serve as media for preparation of emeraldine base PANI dispersions. In this work, the dispersion ability and reversibility of the PANI's redox reactions at its emeraldine state was used as an advantage for one pot preparation of EB-PANI/rGO homogeneous dispersions in DMF solvent. In order to achieve higher conductivities, final PANI-containing electrospun mats were oxidized in mild acid solution so that ES-PANI would be restored inside the structure.

1.4. Poly(Vinyl Alcohol) and Relative High Performance Nanocomposites

Poly(vinyl alcohol) (PVA), the biocompatible product of poly(vinyl acetate) hydrolysis, was reported to be one of the most reliable bio-degradable synthetic polymers for different applications [22]. As one of the most important precursors in bio-compatible

materials preparation, it has been reported that PVA shows interesting performance in different applications such as enzyme carrier composites [22], and transparent electrode membranes [23]. Considering PVA's low mechanical, thermal stability and electrical conductivity properties the urge to introduce the other components in the structure with higher reinforcement abilities has been reported by different researchers [21, 22].

Aston's research group reported immobilization of tyrosinase enzyme within a sol-gel polymer structure for phenol group detection purposes [24]. A sol-gel media of silica-PVA was mixed with tyrosinase solution. Afterwards, the smart nanocomposite sensors were prepared via electrospinning of the mixture. Fourier-transformed IR spectroscopy was conducted for evaluation of enzyme incorporation in the fibrous structure. A noticeable change in Raman spectra of nanofibers exposed to an extremely controlled and monitored phenolic reaction provided the proof of successful operation of as-spun fibers in sensing application.

Preparation PVA/graphene transparent electrodes and their relative electrical properties study was presented by Rajendran and co-workers [25]. The graphite exfoliation was conducted via Hummer's modified oxidation method followed by mechanical exfoliation of as-prepared GO through numerous centrifugation and re-dispersion of GO powder in deionized water by using aggressive ultrasonic probe sonication. The electrical conductivity values of nanocomposites prepared via electrospinning of GO/PVA suspension was improved by 3 times fold by increasing the GO compartment ratio. Although the mentioned relative conductivity values were at order of 10μS/cm, the expected operation improvement with increase in GO concentration was confirmed by EIS analysis.

1.5. Nanocomposite Preparation Processes

In order to increase the nanocomposite properties, two major conventional approaches have been suggested. Firstly the mechanical and thermal properties of PVA were reported to be increased via hydrogel formation [26]. This goal was achieved by use of dimethylformamide (DMF) as co-solvent to the main aqueous solution. This special combination of solvents, not only lowered the total vapor pressure of solution, but also produced physically stabilized hydrogel with hydroxide bonding between DMF and PVA chains. The second method to increase composite properties was to add filler materials with higher characteristics [8, 27-29]. The optimization of nanocomposite

recipe in terms of the compartment composition percentages is crucial for both of the mentioned routes. Although synergistic effect of combining these methods in the final material properties is anticipated, there was no record of pursuing the complex method. The material to be obtained can be beneficial from both the hydrogel formation among polar co-solvents and PVA as well as perfect dispersion of filler material.

Electrospinning is a convenient method for preparing the nanoscale composite materials. To prepare the anisotropic fibers with different functionalities with both random and universal direction of orientations can be easily achieved via electrospinning. This way of preparing nanocomposites with ability of obtaining nanometer scale nonwoven fibrous structure was shown to be one of the most reliable methods among nanocomposite preparation techniques for its ease of performance, rapid manufacturing, process flexibility and low cost of assembly [2-4, 7, 30]. Because of the hardship in achieving homogeneous dispersion of thermally reduced graphite oxide (rGO) in aqueous solutions, effective concentration of filler material in hydrophilic matrix media was not achieved via electrospinning process [11, 28].

1.6. Introduction to Our Study, Necessity of Investigation, Approach Description, and Remarks of Novelty

The incorporation of graphite derivatives, such as reduced graphene oxide (rGO), into aqueous polymer solutions have been reported to introduce a noticeable improvement in overall properties of the resulting nanocomposite material under operation. The constructive effect of graphene addition was particularly reported to be tremendously crucial in the fields of ultrasensitive sensors and catalyst support applications. However, to the date a comprehensive systematic investigation on the defining characteristics of such nanocomposites with respect to material compositions for a special, yet easy to obtain, type of graphene without any functional groups was not reported among literature

Although recently there has been numerous reports, such as Barzegar and co-workers [22] study on hollowness of rGO containing fibrous structures, for the first time the mentioned morphological feature was thoroughly studied via Focused Ion Beam (FIB) analysis. Finally, in order to present a comprehensive study on the prepared mats, morphological, mechanical, and thermal investigations were conducted on the specimens. Fiber alignment effect combined with polymer chain crystallization studies

were used to present better interpretation of the observed specimen mechanical behaviors, respectively.

In our work PVA/rGO and tri-component PVA/PANI/rGO nanofibers were prepared through electrospinning process. For the first time, addition of filler material, to the matrix media was performed via use of the co-solvent as a dispersing agent. The effect of co-solvent addition in final composite's mechanical and thermal properties increase was then observed. This improvement was a result of hydrogel formation of DMF and PVA as the core parts of fibrous structures. The other beneficial effect being observed by this approach was the dispersing role of hydrogen bond interactions between DMF and PVA side groups. Thus, the dispersion quality of rGO faced further improvement. By the proposed method, relatively higher concentrations, up to 2 wt% in dry product, of thermally reduced graphene oxide with effective incorporation in a hydrophilic matrix was achieved.

As a novel study, extensional viscosity analysis was used as an index of solution behavior under electrospinning process conditions. The effect of additive materials, hydrogel forming co-solvent, DMF, and rGO, as 2D filler, on suspension properties such as apparent viscosity and normalized diameter breakdown time was investigated. This modulation of suspension column behavior under constant tension force can show the integrity and quality consistency of solution jet behavior under similar process conditions such as electrospinning.

2. Materials and Methods

2.1. Materials

N, N-dimethylformamide, graphite flakes, poly (vinyl alcohol) (average M.W. 89000-98000 g/mole), aniline monomer, ammonium persulfate (APS), $KMnO_4$, H_2SO_4, H_3PO_4, HCl, H_2O_2, glutarladehyde (25% aqueous solution) (GA), and Ethanol were purchased from Sigma-Aldrich and used with no further purification.

2.2. Graphite Oxide Synthesis

Graphite oxide (GO) was prepared via an improved method published by Marcano and co-workers [1]. During this procedure, a mixture of 3 grams of graphite flakes, and 18 grams of $KMnO_4$ was initially prepared. The process was followed by slow addition of a 9:1 mixture (400 ml in total) H_2SO_4/H_3PO_4 to the reaction vessel kept in an ice/water bath over 15 minutes. The media was then heated up to 50°C and followed by overnight stirring at constant temperature.

The reaction was terminated by addition of the reaction media onto a mixture of 400 ml ice and 20 ml H_2O_2. The mixture was first diluted by addition of DI water up to 1L volume. Afterwards, the mixture was put at rest in ice/water bath for 4 hours until its dark brown color changes to light yellow. In order to achieve better exfoliation and acid reaction the media was then mixed with 1L of a 10 wt% aqueous solution of HCl. Following the mechanical mixing for 30 minutes, the initial solution was centrifuged at 10000 rpm speed for 3 hours.

The complete removal of oxidizing components from GO dispersion was achieved via an extensive washing process, during which the GO was dispersed in ethanol (10 v/v% aqueous solution) and DI water, respectively, followed by centrifugation and removal of supernatant liquid for several times. The final graphite oxide product was dried in vacuum oven for 24 hours.

2.3. Reduced Graphite Oxide Synthesis

Thermally reduced graphite oxide (rGO) was then prepared via thermal exfoliation of graphite oxide using a tubular furnace system in quartz tubes. During that process, the isothermal step was set at 1000°C for 12 minutes. The resulting thermally reduced graphene oxide material was used without further treatment.

The quality of both GO and rGO products were evaluated by Raman and X-ray diffraction (XRD) analyses.

2.4. Synthesis of Polyaniline

Polyaniline (PANI) nanofibers were synthesized using rapid mixing method. First, 0.004 mole of aniline dissolved in 50 mL of 1M HCl at room temperature. 0.1 mmole p-phenylenediamine, as initiator, dissolved in certain amount of methanol at room temperature and was added to aniline solution under constant stirring for 1 hour. Then, in another beaker, 0.001 mole of APS dissolved in 50 mL of 1M HCl at room temperature and stirred for 0.5 hour. The two solutions were mixed with each other in one step without further agitation. Final solution was left for 24 hours in room temperature for polymerization. After 24 hours, the resulting green powder (emeraldine salt) was washed with pH=2.5 HCl acid solution and centrifuged 4 times at 5000 rpm. Supernatant colloidal suspension of last centrifuge step which was stable for 1 week was used for characterizations and also fabrication of nanocomposite.

As the emeraldine salt state of PANI has poor dispersion quality in aqueous media, de-doping of the material was conducted. During the process, the aqueous dispersion of PANI nanoparticles at ES state was titrated by 1M NaOH solution and then its pH value was measured continuously. The process was continued until the pH reached to 10 and the green color of the media turned into dark purple. This visual result indicated that the PANI nanofibers have been de-doped and reached the EB state.

The dispersion was then dried and EB-PANI was collected. In order to eliminate NaCl salt formed during the process, the PANI powders were dispersed in DI water via sonication bath. The process was followed by centrifugation and collecting the decadent PANI nanoparticles.

2.5. Electrospinning Suspension Preparation

In order to obtain a homogeneous dispersion of additive materials in the media, the following process was conducted. In the case of tri-component fibers with PANI introduced, certain amounts of PANI was also added along with the rGO during the first step.

The electrospinning suspension was prepared via a three-step process as follows. (i) Certain amount of rGO (Table 1) was added to 3.11 mL of DMF. The rGO dispersion

was then prepared via ultrasonic dispersing in a homogenizing bath for 24 hours. (ii) A 16.67 w/v PVA aqueous solution in DI was prepared by heating up its mixture up to 70°C for 8 hours. (iii) 8 ml of PVA solution was added to DMF/rGO suspension followed by stirring for 30 minutes. The final polymer concentration was 12 w/v% with respect to total solvents volume. As control samples, two suspensions of neat PVA solution, one with DI water as sole solvent and one with DMF introduced to media as co-solvent, were prepared.

In order to have the best interpretation of sample properties, they were categorized into two categories. Those with up to 0.6% graphene contents were regarded as low-content samples, while those with higher filler concentrations categorized into the high-content ones.

In the case of tri-component fibers with PANI introduced, certain amounts of PANI was also added along with the rGO during the first step (Table 2). The rest of the process was kept similar to the previous experiments.

Table 1 Suspension Composition of PVA/rGO Electrospun Mats (W: water, D: DMF used in samples)

Sample	rGO Content (wt/wt%)[1]	Solvent(s)
WG0	0	DI water
WDG0	0	DI water/DMF
G0.2	0.2	DI water/DMF
G0.4	0.4	DI water/DMF
G0.6	0.6	DI water/DMF
G0.8	0.8	DI water/DMF
G1	1	DI water/DMF
G2	2	DI water/DMF

2.6. Electrospinning

After a number of trial experiments, the optimized set of conditions for electrospinning was achieved. The electrospinning suspension was conveyed via an electrical pump with adjustable speed using a common-use 5mL plastic syringe. The flow rate was kept

[1] The rGO content was calculated as wt% of PVA in dried sample.

constant at 4.2 µl.min^{-1} and 3.2 µl.min^{-1} for PVA/rGO and PVA/PANI/rGO suspensions, respectively.

The electric voltage was also optimized and kept constant at 10kV for all of the samples. The electrospun fibers were collected on an aluminum foil-covered rectangular plate collector. The collector diameters were 15×15 cm^2. The needle tip-to-collector distance was also kept at its desirable constant value of 14 cm.

Table 2 Suspension Composition of Tri-component PVA/rGO/PANI Electrospun Mats

Sample	rGO Content (wt/wt %)	PANI Content (wt/wt %)
G0P1	0	1
G0P2.5	0	2.5
G0P4	0	4
G1P1	1	1
G1P2.5	1	2.5
G1P4	1	4
G2P1	2	1
G2P2.5	2	2.5
G2P4	2	4

2.7. Post-spinning Treatments on Tri-component PVA/rGO/PANI Fibrous Mats

In order to achieve higher electrical conductivity, tri-component electrospun mats were treated through two different approaches.

2.7.1. Cross-linking/Acid Doping

During this treatment, a two-step process, including (i) cross-linking of the mats, and [1] doping of incorporated PANI with acid aqueous solution, was done on the as-spun mats. The detailed information about the procedure of each step is as follows.

2.7.1.1. Cross-linking of The Mats

In order to cross-link the mats, an approach suggested by Chu and co-workers were pursued [2]. During this process an approximately 26mL master-batch solution of

0.15M glutaraldehyde in acetone was prepared. In order to achieve better cross-linking quality, a few droplets of HCl was added. The concentration of the acid in the media was 0.05M.

Afterwards, as-spun mats were immersed into the solution and kept at room temperature for 1 hour. The cross-linked mats were then washed via rinsing DI-water and dried in vacuum oven for 24 hours at 50˚C. (Fig.2)

2.7.1.2. Acid-Doping of Cross-linked Mats

The solution used for acid doping of PANI nanoparticles incorporated into the cross-linked mats was 1 wt% aqueous solution of HCl. This acid was chosen to provide larger size ions with higher probability of entrapment in the cross-linked bulk of fibers, thus resulting in more desirable re-doping of EB-PANI incorporated in the structure.

The doping was conducted through immersion of the cross-linked mats into the solution for 1 hour at room temperature. Afterwards, the excess acid was removed from the mats via washing the doped mats with DI water. Finally, the mats were dried in oven for 24 hours at 50˚C.

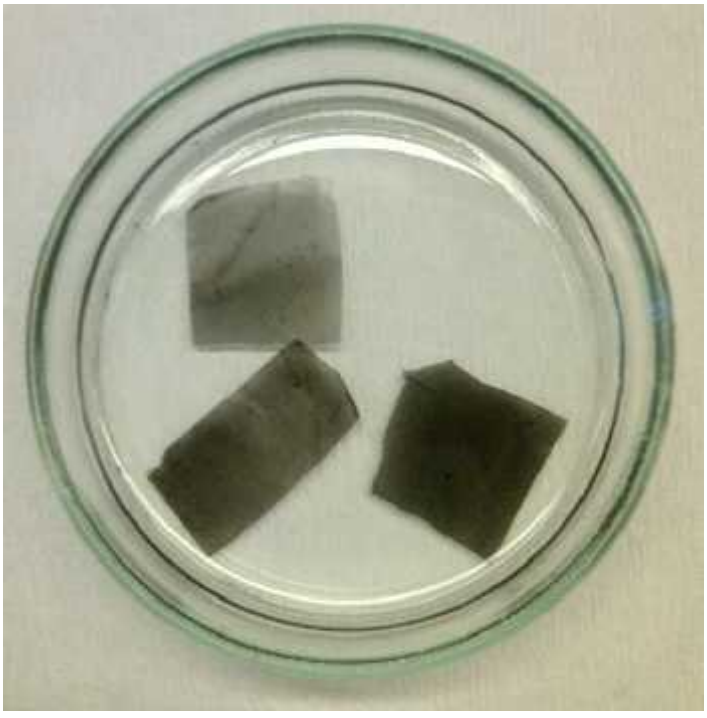

Figure 2 The Electrospun Mats Being Cross-linked and Doped with Acid via Immersion Process.

2.7.2. Thermal Treatment of The Electrospun Mats

Pursuing the goals of partial elimination of the electrically insulating PVA matrix, as well as doping the embedded emeraldine base PANI via mild annealing, the thermal treatment was conducted. After optimizing the process, the process was taken place in a quartz tube in cylindrical furnace. In order to prevent calcination the argon atmosphere was chosen. The heating profile was set to go through a $10^{\circ}C.min^{-1}$ heating ramp up to 220˚C followed by an isotherm step at that temperature for 10 minutes. The digital image of samples prepared for thermal treatment can be found in Fig. 3.

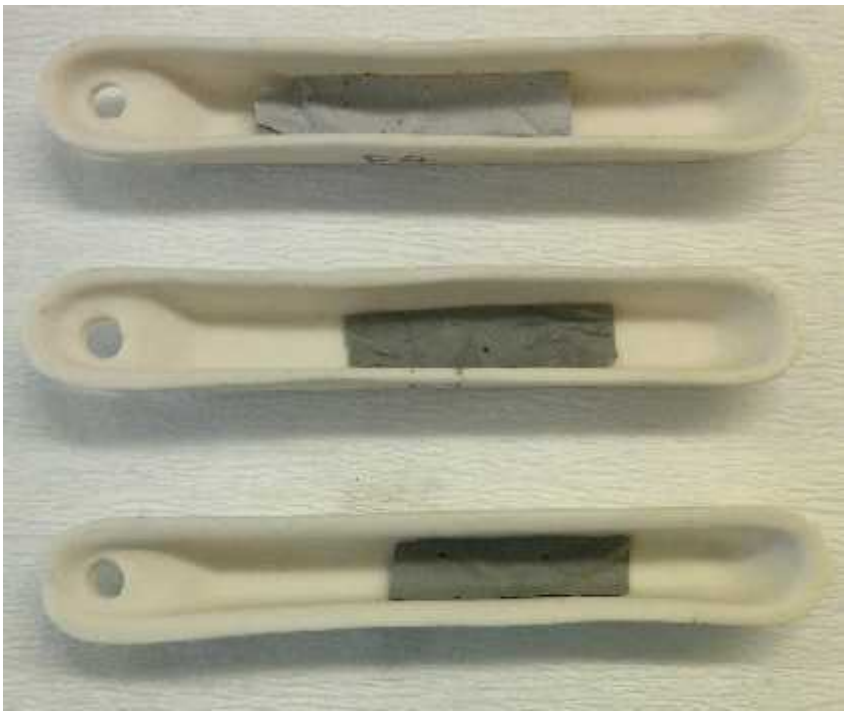

Figure 3 Thermal Treatment Samples Prepared for Thermal Treatment in the Alumina Furnace Cuvettes

2.8. Characterization and Analysis Methods

2.8.1. Suspension Rheology Analysis

As prepared PVA/rGO electrospinning suspensions were examined using a Thermo Scientific ® Haake ® -CaBER ® 1 Capillary Breakup Extensional Rheometer. The information about the change in the apparent viscosity and normalized suspension column diameter with respect to strain rate and time studied, respectively.

2.8.2. UTM Analysis

The Mechanical properties of as-spun PVA/rGO mats were studied by a UTM device. The grip set was chosen for such measurements was consisted of pressurized elastomeric grips, suitable for thin films. A thin film sample compatible load cell of 200N capacity was used for the tension measurements. For each sample 5 respective specimens of 50x20mm^2 dimensions was directly cut from the mats. The samples were further trimmed at their edges in order to prevent any stress concentration zone appearance.

2.8.3. Microscopy Analyses

Fibers were cut using the focused ion beam (FIB) device in order to provide access to the interior texture of the structure. A scanning electron microscopy imaging (SEM) was conducted to study surface texture as well as interior structure of fibers. This analysis was also used for average fiber diameter measurements via Image J software. Transmission electron microscopy [22] provided to further confirm the location of rGO in the fiber structures. Additionally via both FIB and TEM studies hollowness of as-spun fibers were investigated.

2.8.4. FT-IR Analysis

In order to track the hydrogen bonding effect between PVA and DMF a Thermoscientific® FTIR device was used for measurement. Meanwhile, presence of excess DMF amount, as the toxic solvent, in PVA/rGO samples after drying was studied via this technique.

The cross-linking of TT and CC samples were also studied via this experiment. The confirmation to success in those experiments was achieved by comparing the results with the literature [3].

2.8.5. Conductivity Measurement

A four-point probe pressing device used for electrical conductivity measurement of the tri-component mats. In order to provide proper contact area for the experiments, a thin layer of platinum/palladium was sputter coated through a template on the specimens.

3. Results and Discussion

3.1. rGO Analysis Results

3.1.1. Reduced Graphite Oxide Characterization

The XRD spectra of the GO , and rGO, shows perfect exfoliation of the graphene layers in a way that the relative peak for oxide groups found on graphite oxide layers were completely removed in reduced graphite oxide sample . Another confirmation on the layer exfoliation can be achieved by presence of flat line spectrum at 23-28 degrees indicating existence of oxide groups at the (002) plane of polycrystalline GO structure in the exfoliated state [20] (Fig.4-A).

Raman analysis was used to show the desirable exfoliation of the product in which graphite oxide and reduced graphene oxide show an increase in I_G: I_D peak intensity ratio in TRGO sample in comparison with GO from 0.97 and 1.03. It can be concluded from these values that the interlayer spacing, as a sign of material exfoliation, was greatly increased (Fig.4-B) [1, 11].

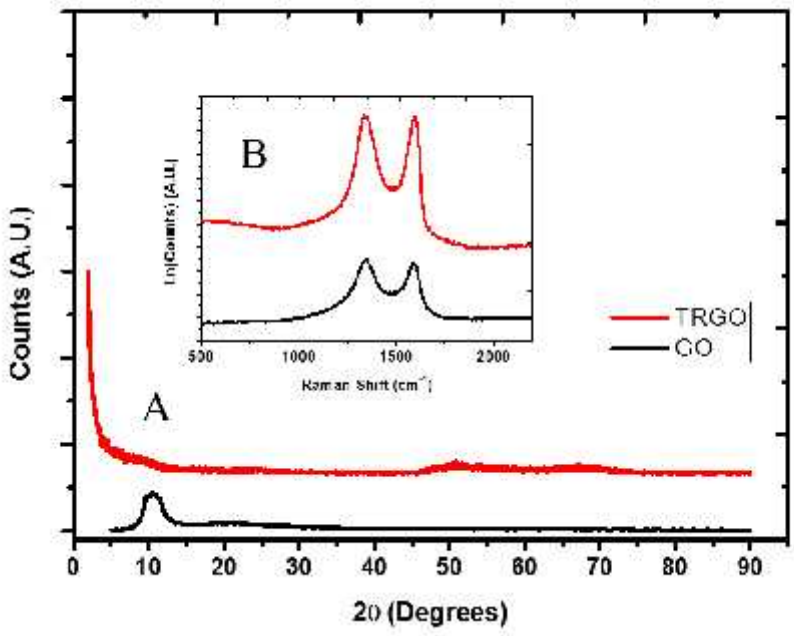

Figure 4 A) XRD Analysis, and B) Raman Analysis Spectra of GO and rGO

The SEM image in Figure 5-A and 3-B show graphite oxide and reduced graphite oxide and their layered structures being changed from a packed form in GO ,where the

individual layers were hardly detected, towards the rGO structure with a well-expanded layer formation with explicit borderlines between the related graphene layers.

The TEM image of the rGO layers (Fig. 5-C) shows them to be transparent indicating enrichment to few layer structured graphene material. It also shows smooth surface without any significant feature or twisted area. This effect results in obtaining a high-surface area filler material. This property resulted in further increase the possibility of achievement of desired polymer/filler interfaces. However, it was shown that the quality of rGO dispersion played an important role to achieve the desired load transfer at the mentioned interfaces.

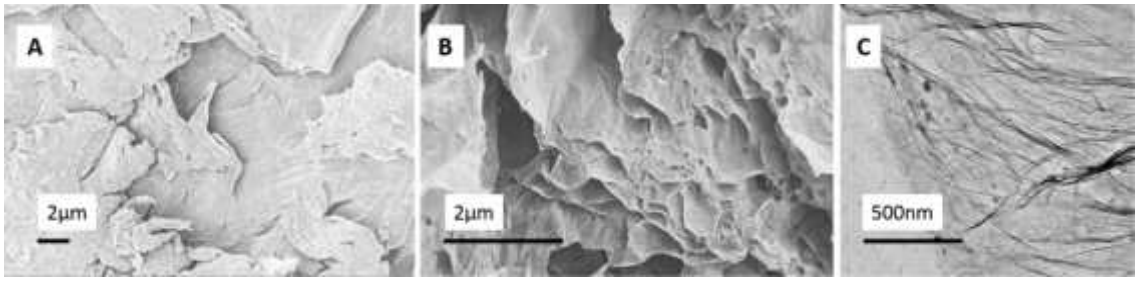

Figure 5 SEM Images of A) GO, B) rGO, and C) TEM Image of rGO

3.2. PVA/rGO Electrospinning Optimization

Pursuing the ultimate goal of obtaining electrospun fibrous nanocomposites containing the highest rGO content possible, a set of experiments was designed and conducted. The 0.3 wt% rGO-content sample (with respect to total dry material's weight) was chosen as the study composition for optimizing the approximate concentration of PVA in the final suspension. 4 levels of PVA concentration (wt/v %) in the electrospinning suspension was chosen for this purpose. The concentrations were 8, 10, 12, and 14 wt/v %, respectively. As it was shown in the electron microscopy image of the 8 wt/v % PVA sample (Fig6-A), the obtained film mostly consisted of spherical shape structures with limited fiber formation. This phenomenon was occurred due to lack of electrospinning jet consistency as a result of low PVA concentration. The PVA also has hydrogen bond interaction with the DMF, as one of the fiber-reinforcing parameters, the shortage in PVA-DMF interaction was the other responsible factor in formation of spherical structures. The increase in polymeric matrix concentration resulted in improvement of fiber formation by adding the jet consistency. As a result at higher concentrations the desired fibrous structure was obtained. However, in the 10 and 14% samples the density of irregular morphology structures, such as graphene clusters and polymer beads, was

higher than 12% sample (Fig. 6-B, D). As a conclusion for this optimization process, the 12 wt/vol% concentration of PVA was chosen to be the initial building block of the rest of design of experiments and sample preparation phases (Fig. 6-C).

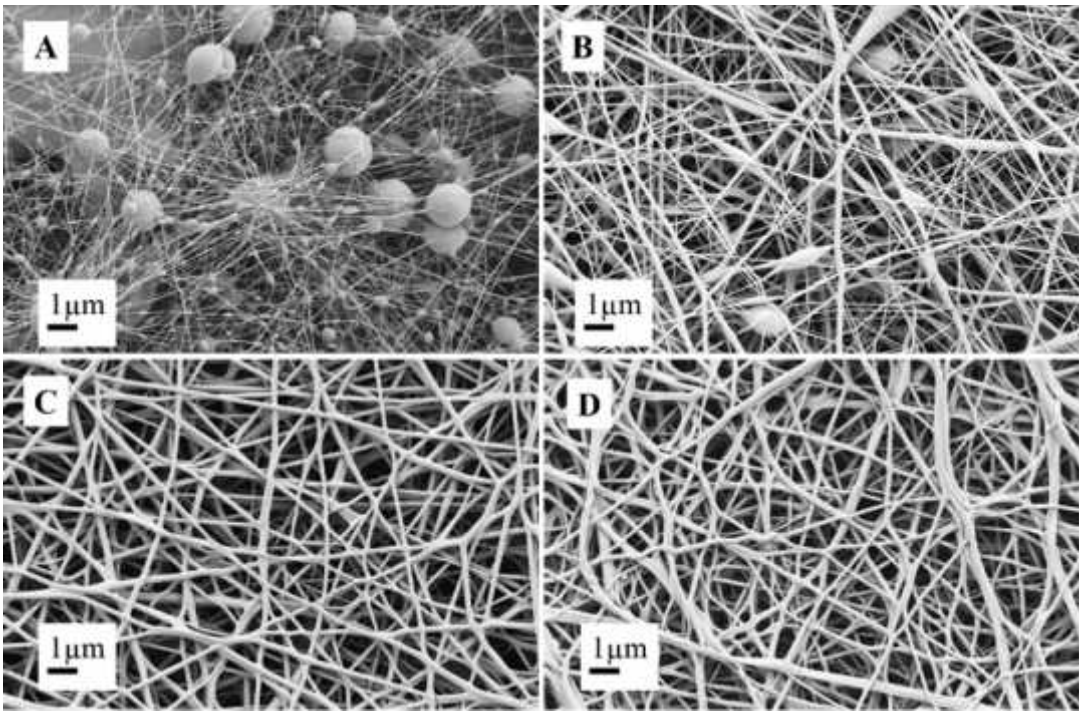

Figure 6 SEM Images of Samples with A)8 wt/v%, B)10 wt/v%, C)12 wt/v%, and D)14 wt/v% PVA Concentration in Solution Media with Constant 0.3 wt% rGO Incorporated With Respect to The Dry Nanocomposite Mass.

3.3. PVA/rGO Electrospun Nanocomposites Characterization

Table 3 Material Composition and Average Diameter of As-spun Mats (W: water, D: DMF as solvents used)

Sample	rGO content (wt/wt% in dry mat)	Co-solvent	Average Diameter (nm)
PW0	0	--	338
PWD0	0	DMF	552
G0.2	0.2	DMF	389
G0.4	0.4	DMF	344
G0.6	0.6	DMF	235
G0.8	0.8	DMF	276
G1	1	DMF	292
G2	2	DMF	275

3.4. Suspension Rheology Analysis

As it was previously reported by different researchers [31], the solution properties have a great effect on finally-obtained fiber microscopic properties, such as morphology,

alignment, and average diameter, as well as macroscopic properties, e.g. thermal and mechanical properties. Extensional viscosity analysis as a novel method for investigation of rheological behavior of suspensions and solutions under constant tension forces, can be used as an index of the suspension behavior during the electrospinning process. This ability of modulation, further assisted the analysis of fluid jet quality and its consistency under similar conditions.

The apparent viscosity change with respect to strain rate for the selected samples (Fig.7-A) shows the effect of hydrogen-bond interaction between DMF, as co-solvent, and PVA chains. The increase in the approximate apparent viscosity values of DMF containing sample (PDW0) signifies that the physical hydrogel formation takes place by time of mixing step among polymer chains and the co-solvent molecules. Thus a local viscosity heterogeneity within the polymer solution occurs. This effect resulted in significant change of fiber interior morphologies in comparison with the pristine aqueous solution of polymer. The viscosity of PWD0, with both DI-water and DMF solvents, sample was recorded as over 2 times-fold higher compared to PW0, with DI-water as sole solvent. This change in solution microstructure, further increased chain movement limitations. Increased apparent viscosity values with respect to strain rate were then concluded to be the result of the mentioned change in chain movement behavior [26].

The effect of graphene incorporation to the suspension was also studied in G1 sample. As the viscosity and overall behavior of solution exhibits no significant change, which can be regarded to low concentration of filler compared to the matrix as well as its decent dispersion benefitted from the perfect interaction of DMF and PVA aqueous solution. Such behavior suggests that the filler addition will not show a noticeable interfere with the polymer solution behavior during the electrospinning process. However, localized graphene clusters with no interaction with polymer solution resulted in formation of viscosity fluctuating regions within the suspension. These regions can become nanometer scale inconsistent regions under applied tangential forces, e.g. electrospinning. Such regions showed their viscosity decreasing behavior in the sample’s viscosity values.

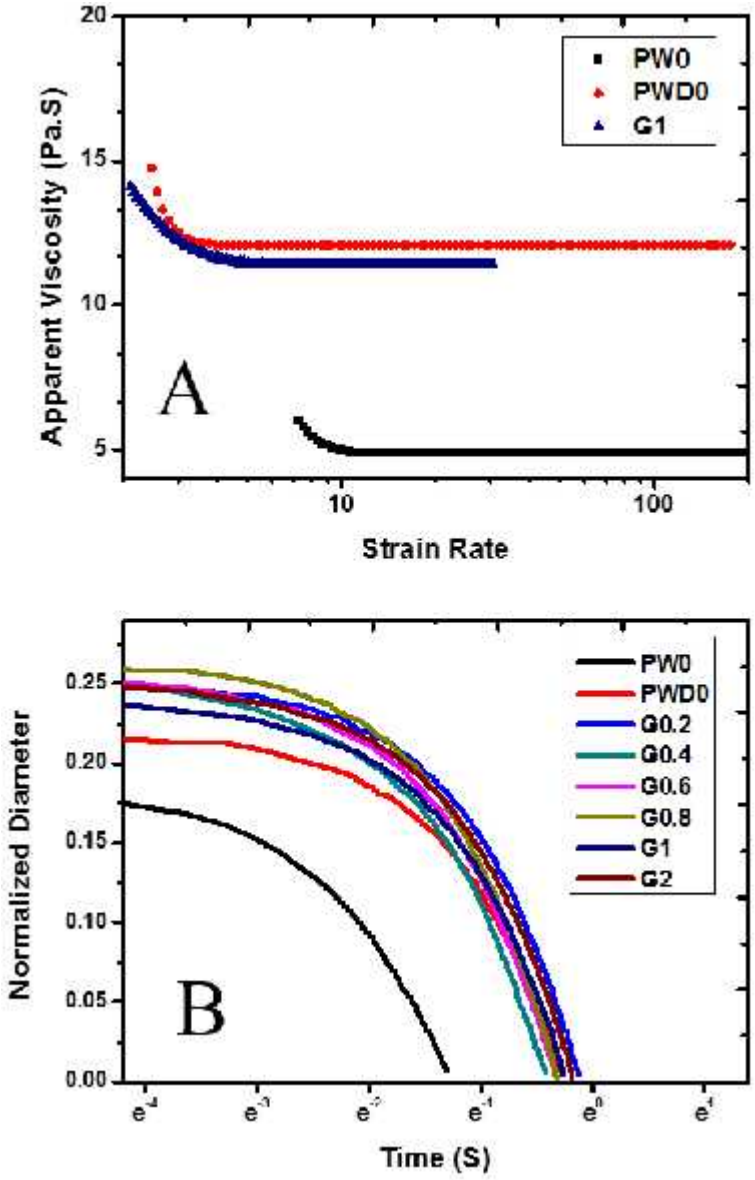

Figure 7 A) Apparent viscosity vs. Strain Rate of PW0, PWD0, and G1 Samples, B) Normalized Diameter vs. Time Graph of All Samples

The other investigation conducted via this analysis was study of the behavior of suspension in terms of normalized fluid diameter with respect to time (Fig. 7-B). As a result of viscosity increase, in DMF containing samples in comparison with PW0 sample the normalized diameter breakup time values were significantly increased. Such behavior is a result of ultimate resistance of the former type of fluid against droplet-breakup phenomenon via formation of high-modulus hydrogel-rich areas. This effect shows that under a constant force, such as the fluid-jet-forming-force application during electrospinning, the graphene-containing samples will have higher jet consistency resulting in further improvement of fiber quality [32].

3.4.1. Fiber Morphology and Diameter Analysis

The SEM images of the as-spun fibers show that at low-graphene concentration samples (Fig. 8 C-E) due to obtaining decent dispersion of graphene clusters within the polymer solution, the fiber morphologies as well as surface textures were almost identical to the pristine polymer samples (Fig. 8-A and B). However, the appearance and density of irregular particles with non-fibrous structures were increased in the high filler content samples (Fig. 8. F-H). This phenomenon was due to lack of success in achieving the desired filler dispersion within the matrix media. In that regard, graphene agglomerations as well as bead-like features were introduced to the mat structures. The morphology consistency was regarded as a parameter reflecting the fluctuations in electrospinning process. Having observed the formation of non-fibrous structures in high filler content samples, it was concluded that poor filler dispersion introduced heterogeneity in the solution, thus process fluctuations were also increased. A closer look to the G2 sample (Fig. 8-I) with highest graphene concentration shows that the mentioned process-fluctuations resulted in formation of series of fibers with varying average diameters.

The increase in fiber diameter values of PWD0 sample is considered as a result of physical hydrogel forming effect of DMF/polymer interactions (Table 1). As it was mentioned during rheology investigation, this effect resulted in higher viscosity values. Thus, the required force to obtain fine fibrous structure was increased. Graphene dispersion introduction to the suspension, as a highly-conductive component, caused further improvement in the induced force with minimal interrupting impact on jet formation. As a result, the fiber diameters showed a decreasing trend with respect to graphene content. However, at higher filler concentrations, such as G1 and G2 sample, due to the presence of filler clusters, the fluctuations during the process will be increased. Local viscosity fluctuations arisen from graphene clusters in the solution consequently resulted in relatively higher fiber diameters as well as irregular morphologies appearance.

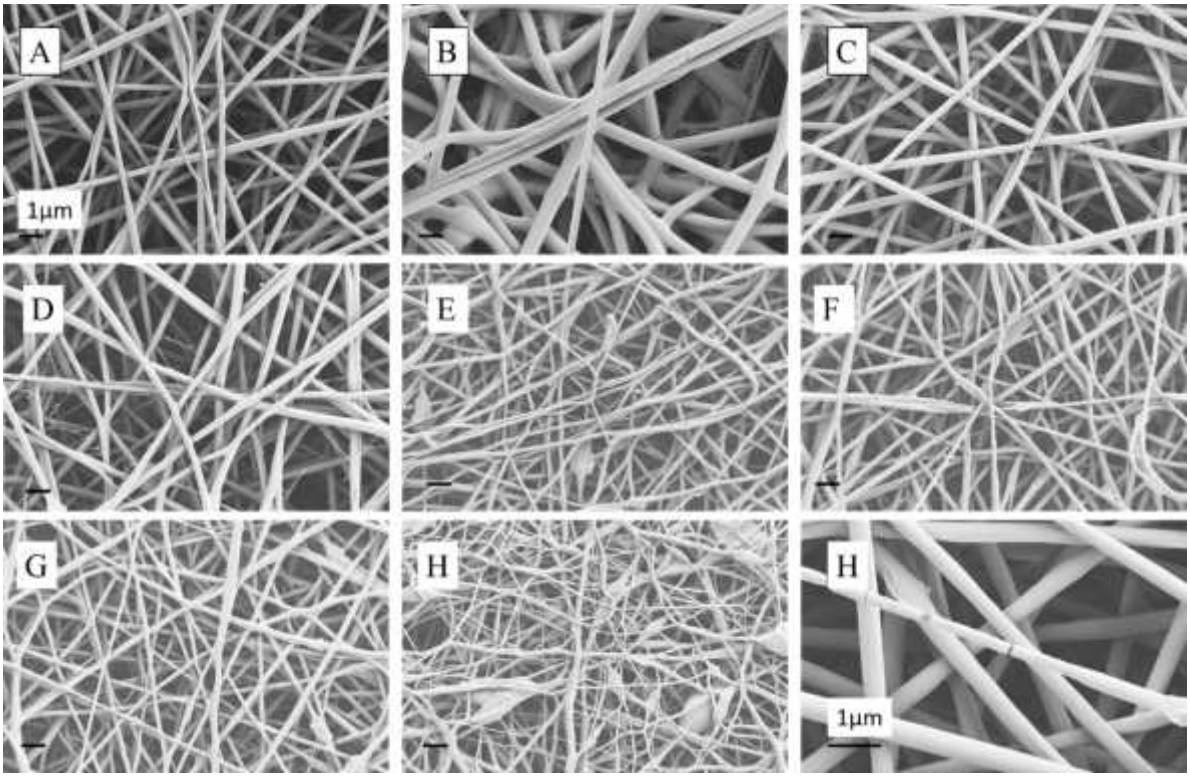

Figure 8 SEM Images of Samples A) PW0, B)PWD0, C) G0.2, D)G0.4, E)G0.6, F)G0.8, G)G1, H)G2 at 20kx Magnification and I) G2 at 50kx Magnification

Since more process disturbance happens by change in viscosity under constant electrospinning conditions, the slight decrease in apparent viscosity values of such samples, showed by their respective rheology investigations, was another parameter defecting the morphology and average fiber diameter of their as-spun mats.

The SEM images of as-spun fibers milled and cut by FIB (Fig. 9) show a noticeable change in interior structure of fibers by incorporation of graphene. As it was shown in pristine sample (PWD0) image in fig.6-A, the fiber structure shows a bulky shape, while in a low graphene content sample (G0.6) the internal structure changes to a hollow one without any difference with pristine sample in terms of fiber surface texture (fig.9-B) [11, 28].

Although, in higher filler concentration samples (G2) irregular morphologies were formed, the hollowness of fibers found to be still intact. The cross-section imaging (fig.9-C) from such non-fibrous structures showed similar features to the pristine fibers.

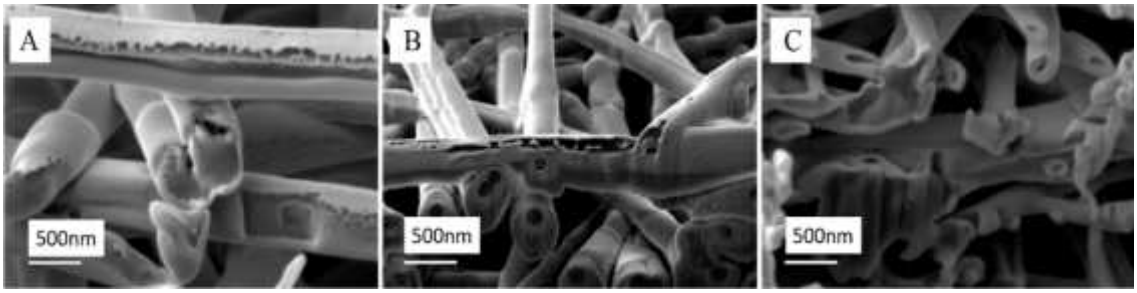

Figure 9 SEM Images of FIB Milled Samples of A) PWD0, B) G0.6, and C) G2

TEM as a perfectly coupled analysis with SEM was conducted. The TEM images shown in Fig. 9 indicate a precise set of information about the interior structure of fibrous structures. As shown in Fig. 9-A, in the pristine samples without any incorporated rGO the fiber morphologies showed no hollowness and a bulky interior structure was observed. The hollow structure was achieved by introduction of rGO in the electrospinning suspension media. It was shown in Fig. 9-B that for G0.6 sample, with 0.6% rGO incorporation with respect to dry material, hollow interior structure was formed within the electrospun mats.

During the TEM study, rGO clusters have been located. Although formation of filler agglomerations have been shown in recent reports[33], our imaging confirmed that graphene-based fillers have been perfectly dispersed in the media as a result of the extensive dispersion process in the DMF co-solvent media. This high quality of polymer-filler interaction was achieved by synergistic effect of stabilizing nature of PVA in interaction with DMF co-solvent. As a result, in Fig.10-C and D, graphene layer-like textures embedded within the fibrous structure were observed indicating that a desirable exfoliation of graphitic layers was also achieved[34]. However, the TEM image of G2 sample (Fig.10-D) shows that the graphene textures occurred at irregular morphology sites of fibers. This effect is a result of cluster formation tendency among graphene layers during the fiber formation.

By comparing the G0.6 and G2 samples TEM images, Fig.10-C and d respectively, an increase in density of graphene layers within their clusters was recorded. Despite the increase in amount of introduced rGO in the suspension media, the consistency in transparency of fibers during the imaging confirms that there is no noticeable increase in number of graphene particles associated in a single rGO cluster.

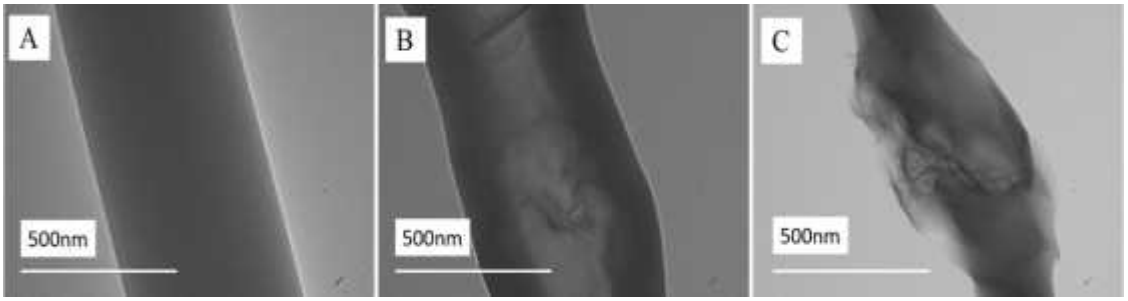

Figure 10 TEM Images of A) PWD0, B) G0.6 Hollow Structure, C) G0.6, and D) G2 rGO Cluster Samples

3.4.2. Thermal Properties of As-spun Fibers

The TGA results shows that the decomposition behavior of the electrospun mats have changed in a reasonable manner due to incorporation of graphene compartment (Fig. 11). The onset temperature for the material decomposition within the P0 sample with no incorporated graphene is recorded as 345°C. By introducing graphene the thermal decomposition temperature was increased by over 20°C for P0.2 where further 60 degrees improvement was shown in higher graphene containing sample behaviors. This effect can also be noticed by studying the remaining mass at 600°C where the highest remainders can be seen at high graphene contents, respectively. This shows the constructive effect of graphene through thermal stability improvement of the fibrous structure [11, 23, 35].

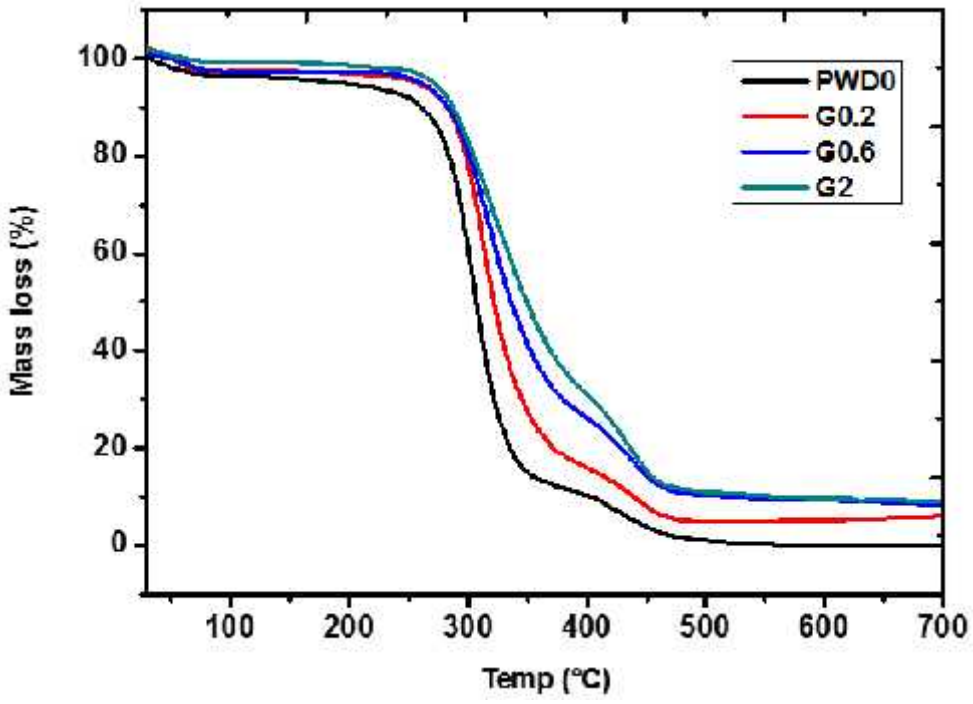

Figure 11 TGA Analysis Graphs of Electrospun Mats

Table 4 TGA Analysis of The Decomposition Temperature Ranges of The Electrospun Mats

Sample	First Decomposition (°C)	Second Decomposition (°C)
PW0	197-286	299-368
PWD0	204-341	341-429
G0.2	289-372	372-486
G0.4	246-398	398-493
G0.6	230-380	380-514
G0.8	259-406	406-527
G1	277-402	402-510
G2	281-395	395-541

3.4.3. Raman Spectroscopy

Raman spectra of the as-spun fibers shows consistency in terms of D and G peaks of graphene layers at 1326 and 1580 cm^{-1} without any shifting or noticeable difference. Such results prove successful incorporation of filler within the fibrous structure (Fig. 12).

In order to study the toxic solvent (DMF) removal from the mats, they were hold in vacuum oven at 30°C overnight. In the Raman spectrum the relative peak of hydroxyl bond between PVA and DMF was mentioned to be detected at Raman shift value of 1440 cm^{-1}[36]. In low graphene content samples this peak can be seen as an explicit shoulder besides the D graphene peak. By increasing the graphene content, as a result of higher fiber stiffness as well as lower fiber merging, the mentioned peak was hardly detected. However, in G2 sample which due to graphene cluster formation, some of the fibers was formed with extremely low graphene incorporation levels, fiber merging takes place and some of the solvent will be trapped inside the structure. The Raman spectrum of G1 sample shows perfect elimination of toxic solvent so the as-spun mat can be used for further biological studies.

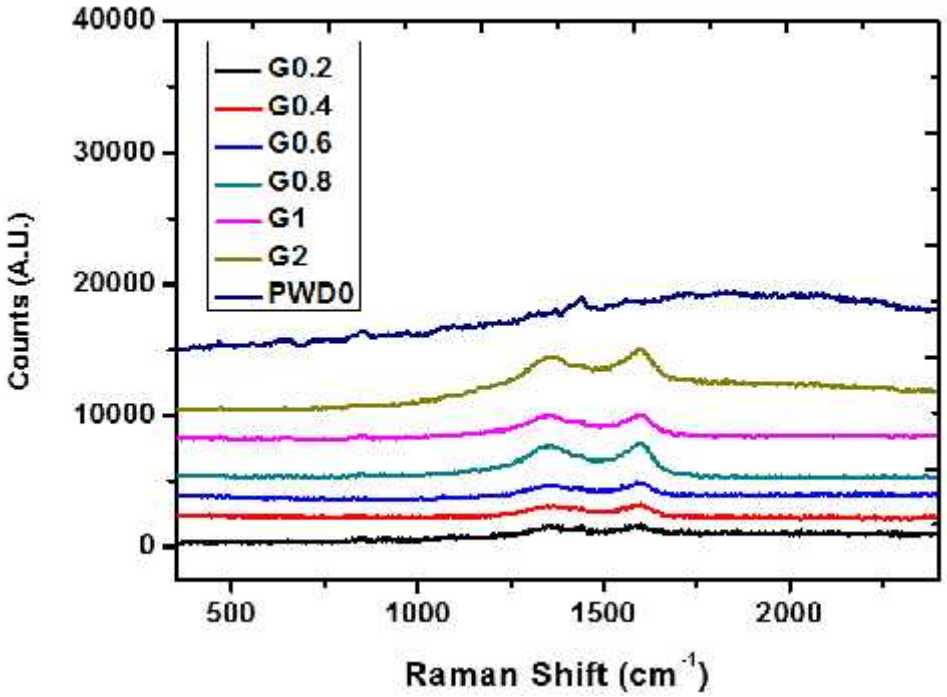

Figure 12 Raman Spectra of As-Spun Mats

3.4.4. FT-IR analysis

The governing parameters in the case of strain at tensile strength are the polymer crystallization as well as graphene cluster alignment. The FT-IR analysis was used to determine the change in crystallinity of polymer chains within the fibers with increase in graphene amount (Fig. 13). The peak at 1144 cm^{-1} was mentioned to be a determining peak for C-O or –OH groups in crystalline regions [23]. Since there was no observed peak-shift for the crystalline regions' peak with respect to graphene content change, the crystallization behavior of as-spun mats was proved to be similar throughout the whole set of samples.

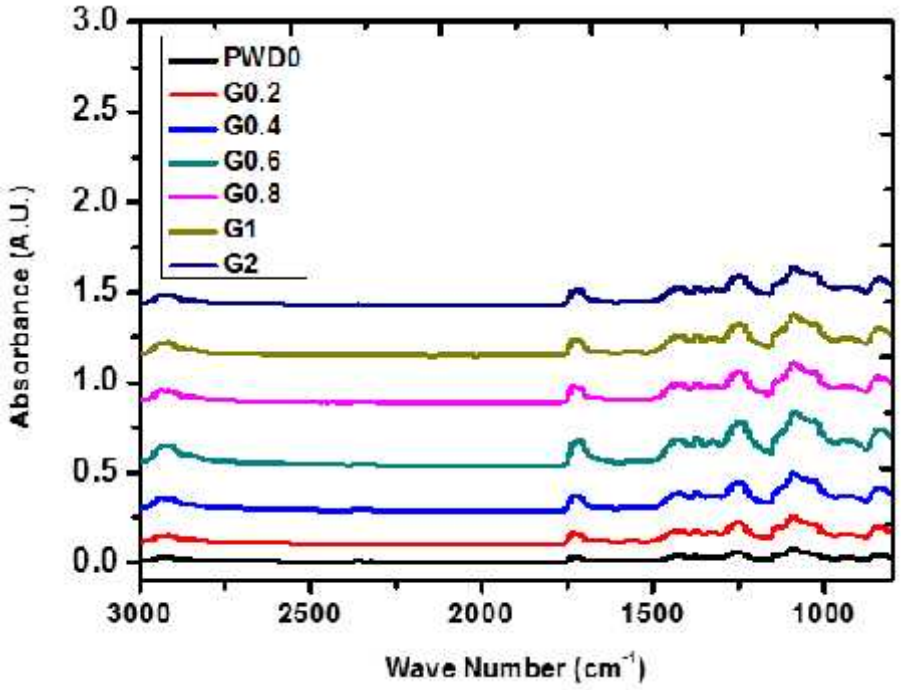

Figure 13 FT-IR Spectra of As-spun Mats

3.4.5. Mechanical Properties

A gradual increase in tensile strength values can be seen by increasing the fiber graphene content (Table. 3). This effect was mentioned to be the result of both constructive polymer/filler interaction as well as the higher stiffness of fibers in low-graphene content samples. However, the synergistic effect of graphene layer alignment among the high concentration mats is found to be responsible for their relatively improved strength.

At low graphene content a desirable dispersion of filler particles was achieved where at higher contents the ultimate dispersion observed was not be as homogeneous as of the lower concentrations. This effect introduced higher levels of either weak polymer-graphene or graphene-graphene interfaces. The irregular morphologies shown in the SEM images of high-concentration samples also confirm the increase in filler-filler interactions. The higher the amount of such interactions, more brittleness behavior will be incorporated within the specimen mechanical properties (Fig.14-C). Although the specimen's macroscopic necking behavior was observed (Fig. 14-D), the responsible phenomenon for such mechanical performance was resulted from the fiber alignment along the load direction (Fig. 14-A, B). While in G0.2 sample, similar to pristine sample, high level of fiber alignment was observed, by increasing the graphene content,

as the brittle component, the fibrous structure remained constant during the drawing process and the fiber alignment behavior showed a dramatic diminishing trend.

The strain at tensile strength recorded value trend was described by this effect, in which for the low-graphene-concentration samples a gradual increasing behavior can be seen, while the high filler content as-spun fibers show an abrupt decrease in terms of the mentioned strain values [10].

The effect of the increase in brittle and weak filler-filler interfaces also provides confirmation for the Young modulus change of the samples in terms of graphene content. The highest modulus was found to be for the G0.6 sample with 103.9 MPa. Within this sample the highest level of constructive polymer-graphene interaction with desirable load transfer ability was observed [10, 23].

Table 5 Mechanical Properties of As-spun Mats

Sample	E modulus (MPa)	Tensile Strength (MPa)	Strain at Tensile Strength (%)
PW0	64.73 ± 5.95	2.97 ± 0.72	283.24 ± 13.93
PWD0	67.12 ± 9.12	3.21 ± 0.61	234.01 ± 8.67
G0.2	69.84 ± 7.66	3.16 ± 0.85	107.05 ± 10.82
G0.4	101.73 ± 4.88	2.95 ± 0.11	153.83 ± 48.09
G0.6	103.98 ± 12.10	3.30 ± 0.09	227.87 ± 23.97
G0.8	91.43 ± 7.50	3.38 ± 0.52	120.38 ± 33.74
G1	87.67 ± 6.93	4.83 ± 0.28	93.37 ± 9.56
G2	85.67 ± 12.51	5.51 ± 0.37	104.03 ± 9.27

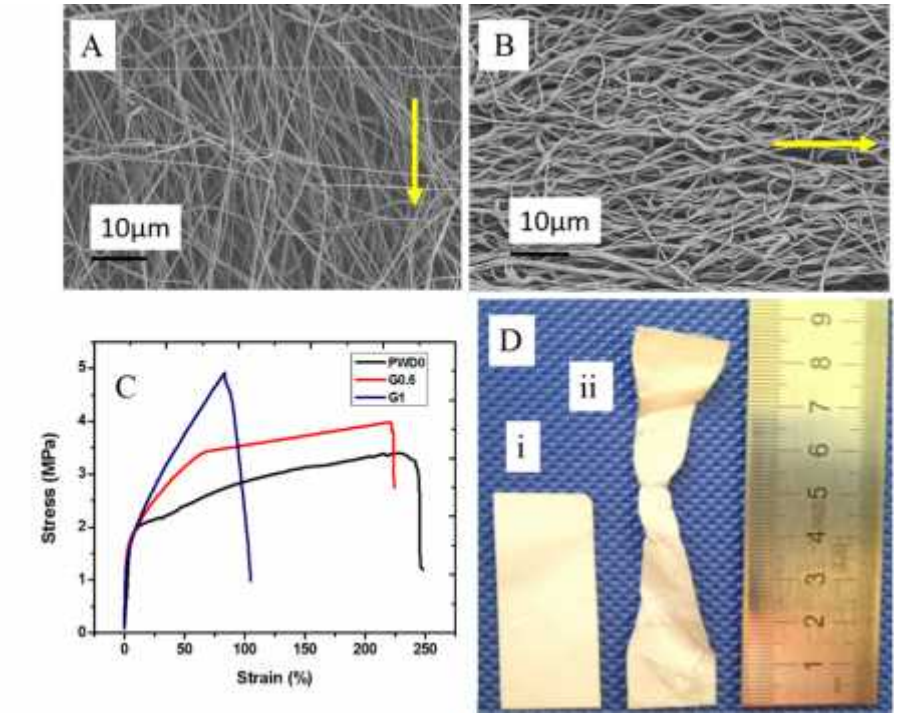

Figure 14 A) SEM Image of Sample PWD0 and B) G0.6, C) Stress-Strain Plot of Electrospun Mats, and D) Digital Image of UTM Specimen i) Before, and ii) After Analysis (The yellow vectors indicate applied load direction)

Magnified illustrations of both the elastic and plastic deformation regions within the UTM analysis graph of as-spun specimens are shown in the figure 15. In the elastic deformation illustration, the graph slope of graphene-containing samples was shown to be at noticeably higher values compared to neat sample, indicating the desirable young's modulus increase expected to be recorded via incorporation of rGO. Relatively lower Young's modulus of high filler-content samples with 1 and 2 wt/wt% of incorporated graphene in comparison with a moderate level of 0.6 wt% incorporation in G0.6 sample was also shown in that graph. The increase in weak filler-filler interaction formation which prevented the desired load transfer among polymer and filler particles from happening was the responsible phenomenon for the mentioned defect. Formation of irregular graphene clusters in high rGO-value samples, shown in their relative SEM images, confirmed the claim mentioned above.

In the plastic deformation area's relative graph, the low graphene-content samples' behavior followed the neat sample's, resulting in formation of a high-strain but low-stiffness behavior regime. The case for high graphene-content specimens were different as in the plastic deformation region, a sudden increase in material stress values was recorded, confirming the formation of a high-stiffness and brittle filler structure in behavior compared to the pristine as well as low filler-content samples. By studying the

average diameter of fibers in the specimens before and after the drawing, it was shown that the average diameter decrease in pristine sample was almost 200 nm, where for graphene-containing samples this value showed a drastic diminishing trend indicating two main results about specimens' microstructure. Firstly, it showed that the increase in brittle behavior of samples under applied tension loads with respect to the increase in rGO amount which resulted high stiffness in fiber behavior yet prevented individual fiber necking to happen. Consequently the strain at breaking point in those samples was decreased from over 250% to around 110% in PWD0 and G2 samples, respectively. Secondly, it was shown that in pristine PVA samples, beside the fiber alignment, microfiber necking phenomenon was the key factor affected the plastic deformation of specimens in macroscopic scale, where the former phenomenon has been found to be responsible for the energy-loss behavior of sample with graphene incorporation.

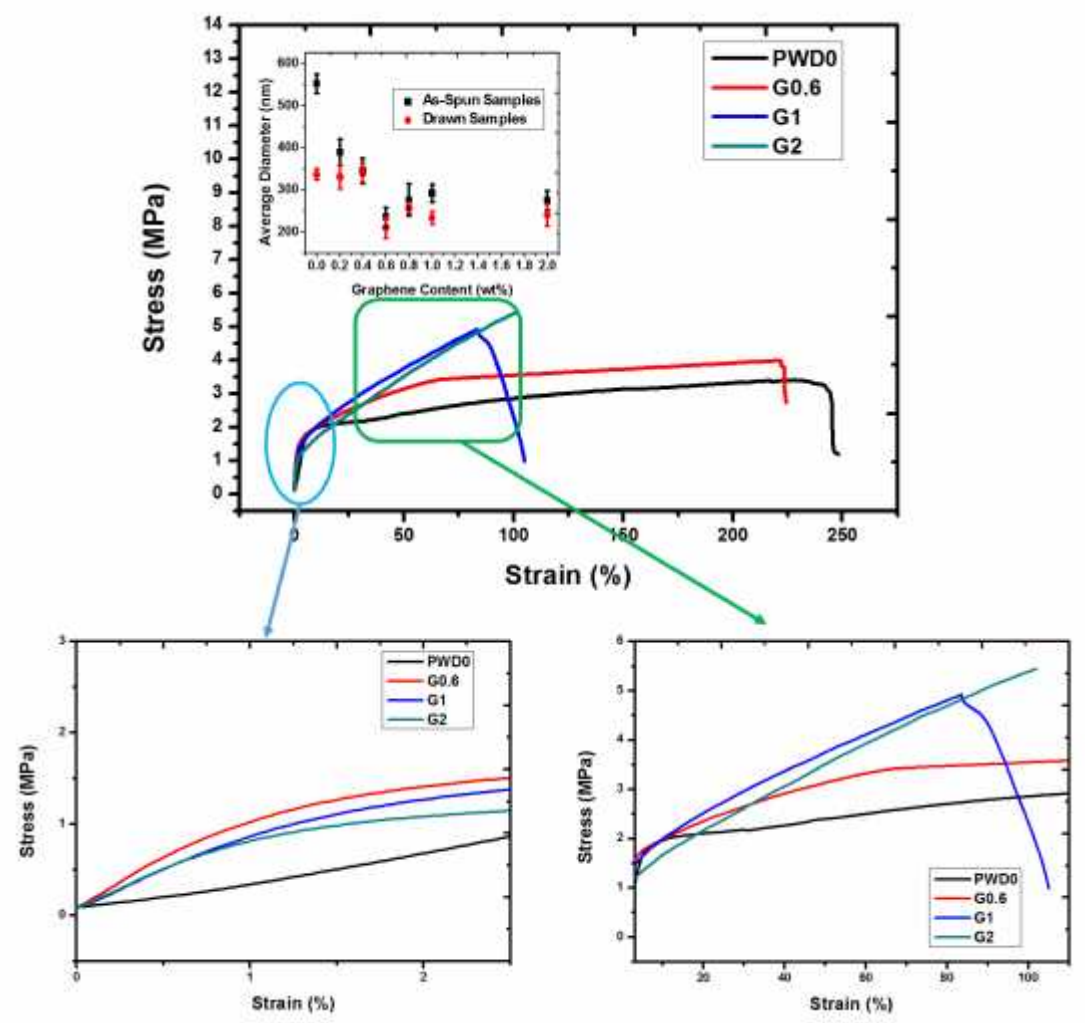

Figure 15 Magnified Stress-Strain Graphs of Specimens at Their Elastic and Plastic Deformation Regions

3.5. PVA/PANI/rGO Electrospun Nanocomposites Characterization

A homogeneous design of experiment for this step of investigation was conducted. Table 4 shows that three levels of concentration for each of the filler materials (rGO and PANI) was considered in the design.

Table 6 Material Composition of Tri-component Electrospun Mats

Sample	DMF: PVA solution*	rGO content (ca. wt/wt % in dry media)	PANI Content (ca. wt/wt% in dry media)
G0P1	1:7	0	1
G0P2.5	1:7	0	2.5
G0P4	1:7	0	4
G1P1	1:7	1	1
G1P2.5	1:7	1	2.5
G1P4	1:7	1	4
G2P1	1:7	2	1
G2P2.5	1:7	2	2.5
G2P4	1:7	2	4

*The approximate PVA concentration was fixed at 12 wt% in electrospinning suspension.

3.5.1. Morphology Study of Tri-component Electrospun Mats

The electrospun mat SEM imaging provided required insight about the relative morphology of as-spun mats. As shown in Fig. 16, the microscopic structure in the first three samples with PANI, as the sole filler material, a ribbon-like structure was observed. Such a flat structure indicates the role of conductive polymer in the process of electrospinning during which, the fibrous structure of the PANI nanoparticles, with isotropic orientations achieved via the effective dispersion, induce the further stretching of the electrospinning jet once it reaches the collector's surface. This phenomenon prevented the fibers from drying in their initial circular-cross-section shape. Therefore the finally obtained mats of those samples had smaller thickness values in comparison with the rGO containing samples. Higher packing of ribbons was also observed as it was expected due to planar shape of the ribbon structure itself [37].

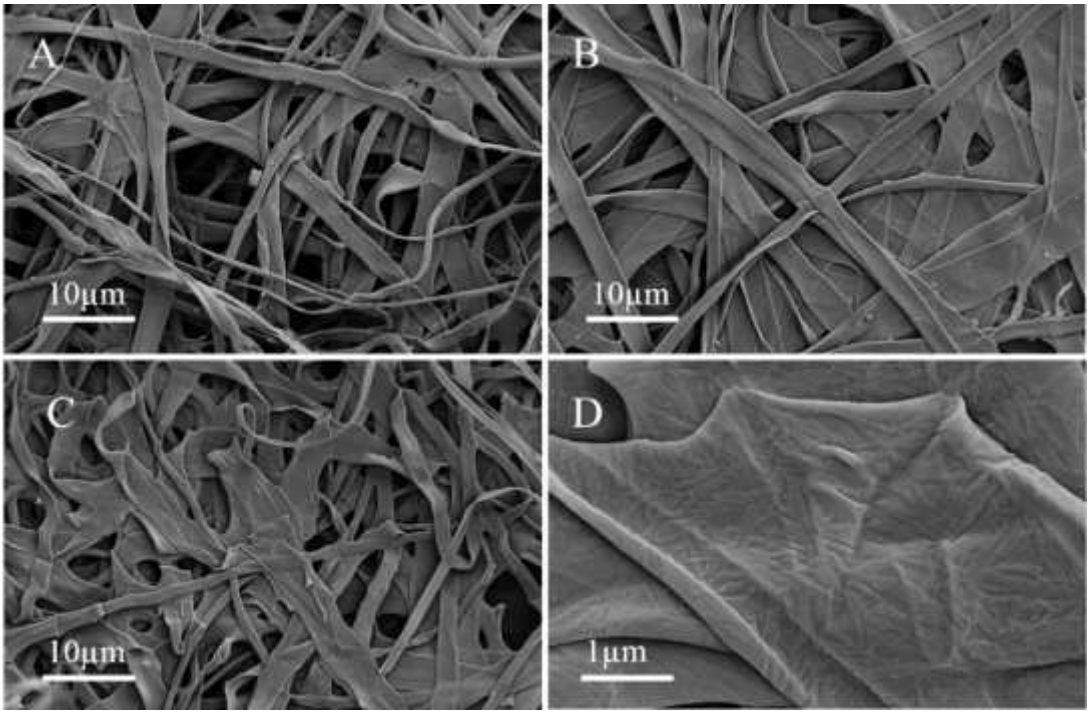

Figure 16 SEM Images of Samples A) G0P1, B) G0P2.5, C) G0P4 at 2kx Magnification and D) G0P4 at 10kx Magnification

The higher thickness of tri-component rGO/PANI/PVA samples, indicated to be the result of rGO incorporation in the material composition. Although the addition of another highly hydrophobic conductive filler added more difficulties to the spinning process, the robustness of fibers have been improved with respect to the increase of incorporated graphene content. The robust fibers formed by electrospinning were dried faster on the collector surface, preventing the structure from collapse. The SEM images of as-spun mats (Fig. 17) confirms the discussion as a transformation trend from the ribbon-like structures to rGO-filled fibrous textures of nanocomposites was shown in the images of rGO-containing samples [38, 39].

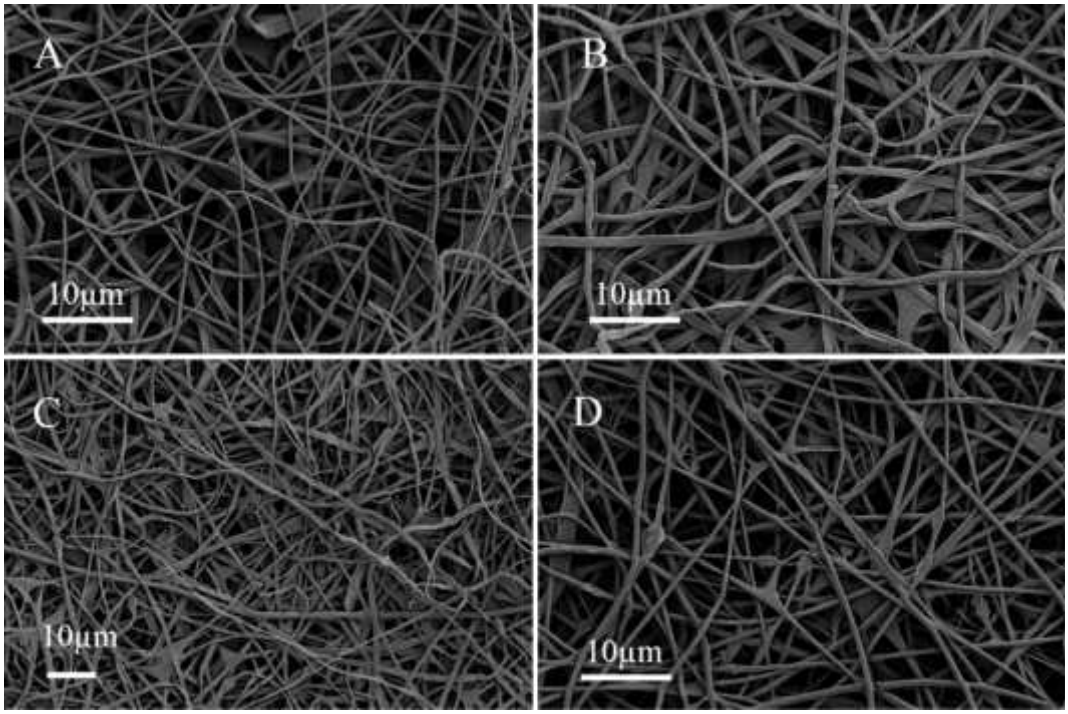

Figure 17 SEM Images of Samples A) G1P1, B) G1P4, C) G2P1, and D) G2P4

In the TEM images of G0P4 sample (Fig 18-A), the formation of aligned PANI nanofiber along the electrospun fiber axis was observed, indicating that the nanofiller-alignment can be achieved via this approach. However, irregular-shape PANI clusters can be seen in the nanocomposite structure. For example a spherical agglomeration of particles was recorded in the sample's TEM image. Formation of the non-aligned structures of embedded PANI is regarded as a result of high conductive polymer content within the nanocomposite composition and the relative fluctuations added to the electrospinning process accordingly [10].

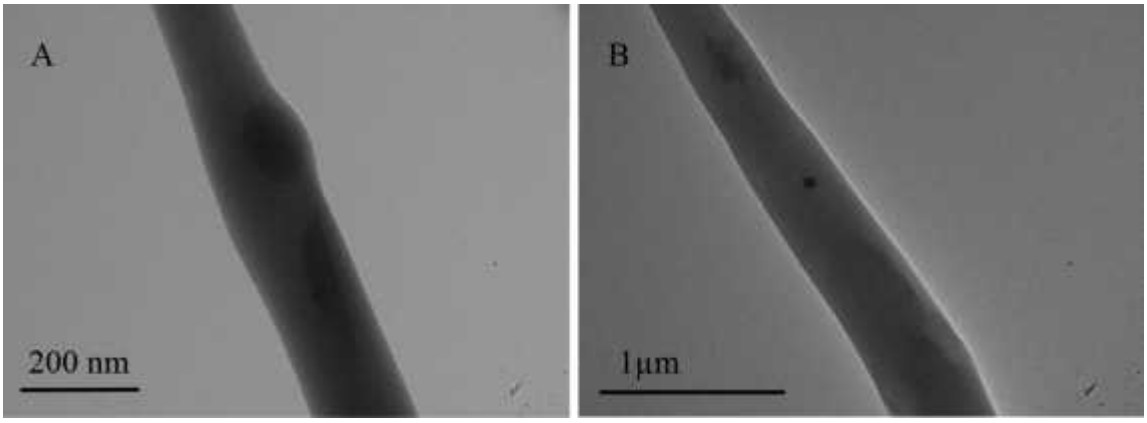

Figure 18 TEM Images of A) G0P4, and B) G2P4 As-spun Fibers Samples

A noticeable change in the diversity of filler structure types recorded in G2P4 sample (Fig 18-B) in comparison with the one with no added rGO filler was observed during

the transmission electron microscopy. Addition of another filler material (rGO) with extremely high mechanical and electrical properties resulted in an increase in the fiber diameter as well as formation of different filler alignment, and placement within the as-spun fibrous nanocomposites. Based on the investigation, features similar to those in the G0P4 sample images was observed that confirmed consistency of PANI fiber alignment in the electrospun fibers. Slightly smaller features with different textures compared to PANI clusters were regarded as the rGO clusters showing relatively more compact morphologies. Such type of aggregation in the rGO nanoparticles was a result of low affinity between hydrophilic matrix and hydrophobic filler material.

3.5.2. Post-Treatment Analysis

3.5.2.1. Cross-linking/Acid Doping

In order to be able to re-dope the incorporated PANI with an aqueous acidic solution, to transform it into emeraldine salt conductive state, a cross-linking step was needed to be performed on the as-spun mats. As it was shown in fig.19 the fibers cross-linked with GA demonstrated a noticeable change in texture as the fibers were merged into each other and formed an inter-connected network. This effect not only improved the mechanical stiffness of prepared mats but also aided the nanocomposite with better contact of embedded PANI and rGO particles between each other. These improvements further enhanced the quality of obtained fibrous nanocomposite in terms of mechanical, electrical, and thermal properties [40].

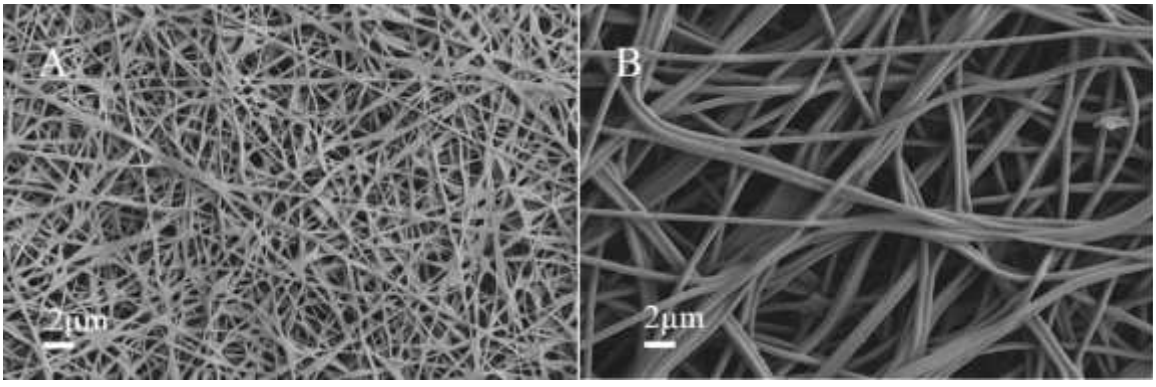

Figure 19 SEM Images of Cross-linked Specimens Prepared From A) G0P2.5, and B) G2P1 Samples, Respectively

Successful cross-linking of the as-spun mats was confirmed by the FT-IR spectroscopy in which the definitive peaks for covalent bonds formed during the process was detected. In the fig. 20, by focusing on detection of the peaks for PVA and GA bonds, at

1085-1150, 1735-1750, 2695-2830, and 3200-3550 cm^{-1} wave number ranges the ether, carboxylic, aldehyde double-peaks, and hydroxyl bonds between PVA and GA was detected, respectively [41]. Thus the successful formation of cross-linking covalent bonds was confirmed by this analysis.

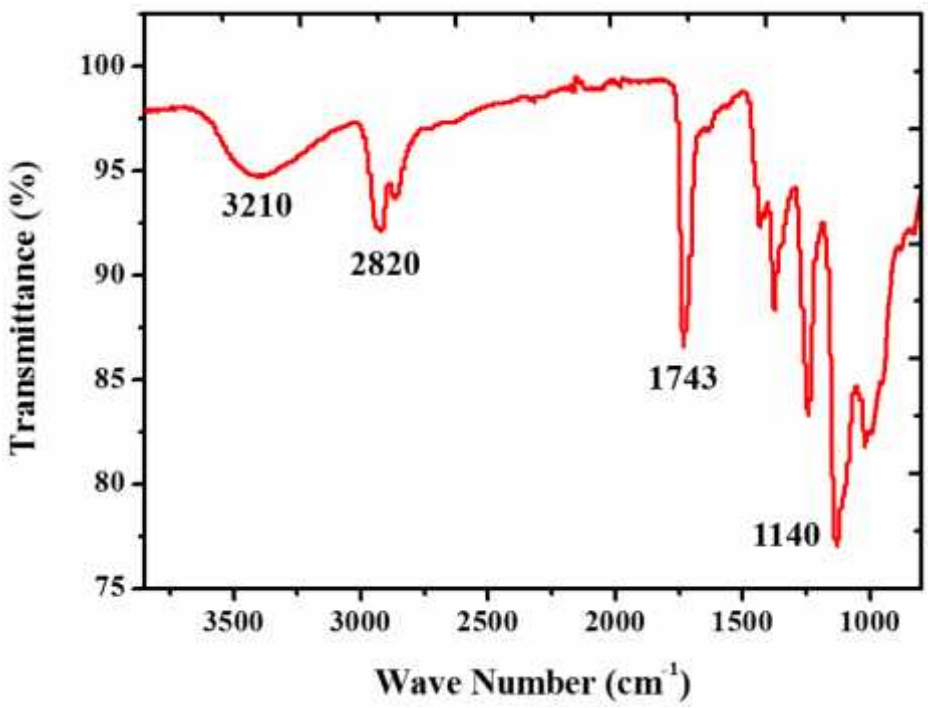

Figure 20 FT-IR Spectrum of Cross-linked and Acid-doped Sample (G1P1)

Additionally, the relative peaks indicating the incorporation of PANI in the nanocomposite structure was also detected. The Emeraldine salt form of PANI showed multiple peaks at 1500, 1338, and 1255 cm^{-1} wave number values. Therefore, the confirmation on incorporation of PANI nanofibers was successfully achieved via this study. However, since the vibrational intensity of EB-PANI was low, the determining peak of PANI's form, at 1750-1650 range was covered by high-intensity PVA and PVA-GA covalent bonds' background [42].

3.5.2.2. Thermal Treatment

TGA analysis as an index of thermal treatment process was conducted on the samples. During the process, which was kept identical to the treatment conditions, a heating ramp followed by the isothermal step all under neutral gas constant purge was executed (Fig. 21). In the respective TGA graph of the experiment it was shown that after a dehydration step at around 100˚C, the mass loss didn't continue until the starting point

of the isothermal step at 220 ˚C. At that region a graph shape was transformed into a decreasing trend behavior indicating the decomposition of PVA matrix. Despite the extensive volume change of as-spun mats after the treatment, both the TGA and FTIR results indicate that most of the matrix fraction remains intact even during the isothermal heating step as the over 90% remaining mass, and high intensity PVA backbone IR peaks was shown, respectively.

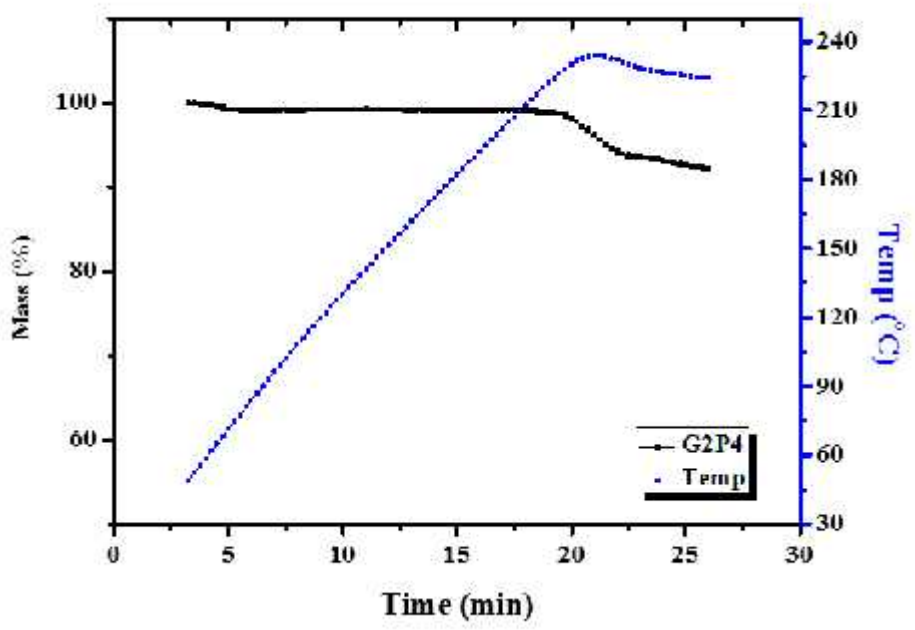

Figure 21 TGA analysis of Thermally Treated Sample (G2P4)

The FT-IR spectroscopy results obtained from thermally treated samples showed two main desired characteristics achieved by means of such a treatment approach. Firstly, a mild cross-link of PVA matrix was achieved and this is due to detection of inter-chain bond peaks at 2650-2890, and 1700-1750 cm^{-1} wave number ranges, respectively [41]. As the second remark of this analysis, desirable thermal doping of PANI through thermal treatment was also validated. The specific peak for emeraldine salt (ES) form among all of the states of PANI, at 1608 cm^{-1} wave number, was reported in the spectrum. The mentioned peak has a low intensity that also matches the previous results of PANI spectroscopy analysis in which the intensity of the spectrum peaks were low (Fig. 22) [42].

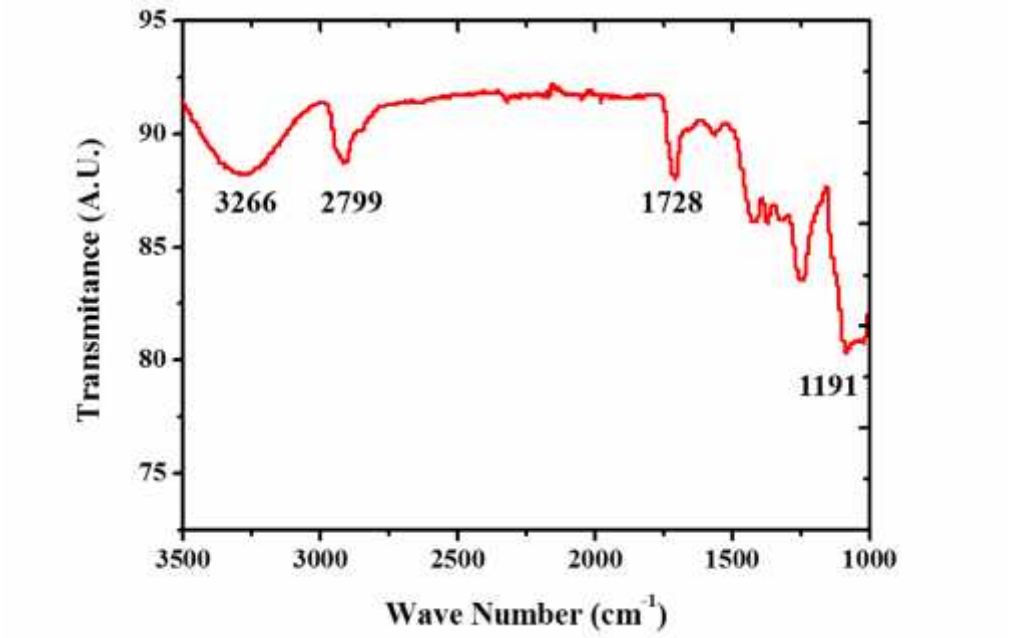

Figure 22 FT-IR Spectrum of Thermally Treated Sample (G1P2.5)

3.5.3. Electrical Conductivity Analysis

The I-V graph of the cross-linked/acid doped samples (Fig. 23-A) shows that by increasing the conductive filler substances the conductivity values was increased approximately over 3 orders of magnitude. The linear plotting of the set of data shows that the specimens behave in a desired linear manner during the operation (Fig. 23-B). Such a behavior was reported to be sign of consistent conducting behavior of the material under a range of applied voltages [43].

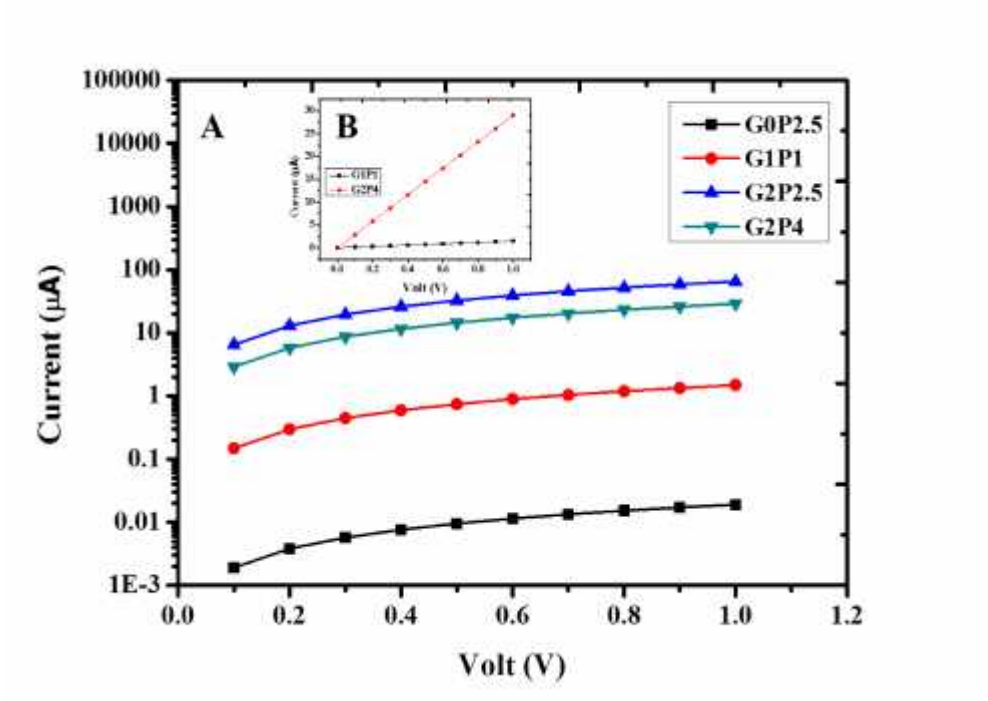

Figure 23 I-V Curves of Cross-linked/Acid-doped Samples Demonstrating A) Increasing Trend of Electrical Properties, and B) The Linear Behavior of Samples Under Applied Voltages

The effect of increase in rGO content was demonstrated to be the key factor in the electrical conductivity of the samples. By following the trend of sample composition change in Fig.23-A, it can be seen that regardless of PANI amount, after each of 1% rGO content-increase levels, the electrical conductivity of samples had reached to at least an order of magnitude higher values compared to samples of previous steps. This phenomenon was shown to be the result of both extremely higher conductivity and specific surface area values of rGO compared to PANI nanofibers, resulting in a noticeable improvement in measured electrical conductivity of the samples (Table. 5). The higher surface area provides a better distribution of PANI as well as enhanced connection of fillers between each other, thus the increase in electrical properties was achieved [43].

Table 7 Electrical Conductivity of Cross-linked/Acid-doped Samples

Sample	Conductivity (μS/cm)
G0P1	0.0035 ± 0.00012
G0P2.5	0.0042 ± 0.00027
G0P4	0.0226 ± 0.00088
G1P1	0.3293 ± 0.0097
G1P2.5	0.7428 ± 0.0116
G1P4	1.5103 ± 0.0073

G2P1	6.8388 ± 0.049
G2P2.5	14.405 ± 0.239
G2P4	6.406 ± 0.0971

While based on the trend of the change in properties it was expected that the sample with highest amount of conductive fillers (G2P4) should show the best performance, the sample containing one level lower amount of PANI had better records in conductivity values by over a time fold comparing the high concentration sample. In the G2P4 sample, the properties were affected by lack of desired filler exfoliation and homogeneous distribution throughout the nanocomposite, further resulting in formation of filler island-like agglomerations along the as-spun fibers. The occurrence of such structures was confirmed earlier by TEM imaging of the mentioned sample (Fig. 18-B). On the contrary by setting the G2P2.5 sample material composition as such, not only high amount of conductive fillers were provided to the electrospinning solution but also the possibility of achieving a more homogeneous dispersion of PANI and rGO in the initial co-solvent by keeping the PANI concentration at the moderate level of 2.5 wt% rather than increasing to higher levels. The well-dispersed distribution of PANI nanofibers was also aided by rGO nanolayers with high available surface area, further improving the network of conductive filler material within this specific nanocomposite structure [43].

The I-V graphs of thermally treated samples show that the lowest electrical conductivity values of attributed samples are at least one order of magnitude higher than those have been cross-linked and treated with acid (Fig. 24-A) . Such further increase in electrical properties was mainly regarded as a result of partial elimination of the insulating PVA matrix due to the mild thermal treatment [43]. The other effective result of the mentioned neutral gas calcination was the merging of electrospun fibers while the filler network remained intact and also the probability of formation of a percolation among networks of fillers in separate electrospun fibers was increased. Formation of a percolation network of fillers embedded inside the nanocomposite was the responsible factor in the general increase in the thermally treated samples' electrical properties in comparison with the acid-doped trials (Table. 6).

Table 8 Electrical Conductivity Values of Thermally Treated Samples

Sample	Conductivity (µS/cm)

G0P1	0.0029 ± 0.00018
G0P2.5	0.0056 ± 0.00093
G0P4	0.0315 ± 0.0051
G1P1	0.1416 ± 0.0049
G1P2.5	0.7003 ± 0.0083
G1P4	1.262 ± 0.063
G2P1	19.06 ± 0.105
G2P2.5	4.827 ± 0.375
G2P4	11.54 ± 0.098

As a similar case of study it was shown that the electrical conductivity has undergone a limited amount of increase with respect to the increase in PANI content at each of the graphene content levels (Table. 6). The range of increase in the studied electrical properties between different rGO concentration-levels are more noticeable where the electrical conductivity of 0.0029 µS/cm in G0P1 sample was increased up to 19.06 µS/cm at G2P1 sample.

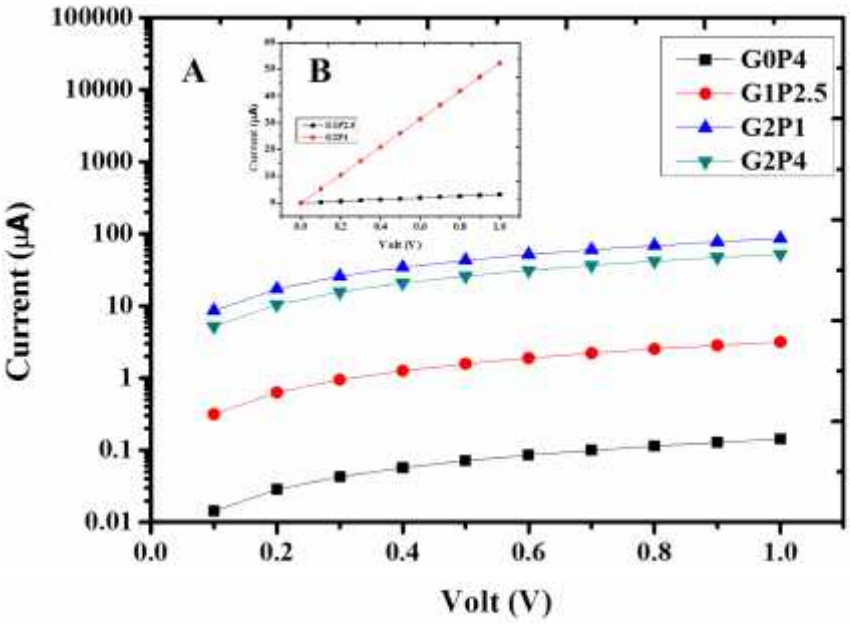

Figure 24 Curves of Cross-linked/Acid-doped Samples Demonstrating A) Increasing Trend of Electrical Properties, and B) The Linear Behavior of Samples Under Applied Voltages

4. Conclusions

During this project graphene oxide was prepared via an improved method based on Hummer's Modified method having numerous advantages compared to conventional methods including elimination of nitrogen oxide pollutant gases, and higher oxidation percentage (in terms of functional group coverage area on layers). Thermal reduction of as-prepared GO was performed under neutral-gas-atmosphere condition and characterization analyses (such as XRD, RAMAN and electron microscopy studies) of obtained product provided confirmation of desirable reduction of graphene layers with no functional groups present in the produced rGO.

Suspensions of rGO in DMF solvent was prepared which was then successfully mixed with PVA solutions resulting in formation a polymer/rGO hydrogel media which was then electrospun to obtain fibrous nanocomposites of PVA/rGO with enhanced mechanical, and thermal properties. During this step, DMF played a key-role as it was used both to provide a suitable media for rGO dispersion as well as hydroxyl-based hydrogel forming agent with the PVA matrix. These attributes of DMF presence in the electrospinning media was proved to have promising impacts of final products' properties.

By FIB/SEM imaging, coupled with transmission electron microscopy formation of clusters of rGO nanosheets within the electrospun mats along with the interior morphological change in as-spun fibers was shown. It was observed that the interior structure of fibers undergoes the change from bulk to hollow structure from pristine PVA samples through rGO-incorporated electrospun samples, respectively.

Improvement in thermal properties of as-spun mats, investigated via TGA/DTA analysis device, were shown to have an increasing trend with respect to increase in incorporated rGO, as heat resistant filler, fraction in their respective electrospinning solution.

Mechanical properties of as-spun mats was studied via a UTM device. The expected increase in mechanical properties (such as Young's modulus and tensile strength) by increase in rGO amount was reported for low-content rGO samples with up to 0.6 wt% incorporated rGO in their structure. However, by further increase in rGO amount, as the brittleness of structure was increased, the Young's modulus and strain at break of the

samples showed a gradual decrease by approximately a times fold in comparison with low rGO-content trials.

By investigating the FTIR spectra of drawn specimens it was shown that there were no noticeable change in crystallinity level of PVA chains with respect to graphene content change. Therefore the effect of polymer chain crystallization during the tension test was considered as negligible in this study.

SEM imaging from the breaking edge of specimens after analysis provided information about the average diameter of fibers after the application of the tension force as well as their alignment towards the load direction. It was concluded that the necking behavior of individual fibers is only present in the pristine samples and in the rGO-containing samples the governing phenomenon found to be level of microscopic alignment of fibers towards the load direction which enforced changes in macro-mechanical properties of as-spun mats.

As the second step of this study successful introduction of Polyaniline into the electrospinning media was achieved and subsequently, the relative electrospun mats were obtained for further treatment and analysis.

SEM and TEM imaging provided information about the morphological texture of as-spun fibers and confirmation of both PANI and rGO in the fiber structure, respectively. It was shown that in samples with no incorporated rGO the morphology changes into a ribbon-like structure where the fibrous structure was regained after incorporation of graphene in the nanocomposite material composition. It was reportedly regarded as the effect of formation of PANI clusters as well as drying holdback induced by the mentioned filler during the spinning process.

In order to improve electrical properties of tri-component PVA/PANI/rGO electrospun mats two different approaches for post spinning treatment was conducted as cross-linking/acid doping and mild thermal annealing. The electrical conductivity of cross-linked/doped samples was increased by an order of magnitude with respect to each level of rGO increase (1 wt/wt%) and approximately 40 time fold higher conductivity at highest graphene concentration. Although PANI was shown to form a percolation network inside the mats, the effect of increase in that compartment fraction ratio was shown to be less than rGO’s on electrical properties.

The thermally treated samples showed an order of magnitude higher electrical conductivity compared to the former type of post treatment samples. However, the overall behavior and the trend of property change with respect to various levels of conductive fillers introduced to media was similar to cross-linked/acid doped samples.

5. References

1. Marcano, D.C., et al., *Improved Synthesis of Graphene Oxide.* ACS Nano, 2010. **4**(8): p. 4806-4814.
2. Biro, L.P., P. Nemes-Incze, and P. Lambin, *Graphene: nanoscale processing and recent applications.* Nanoscale, 2012. **4**(6): p. 1824-1839.
3. Zhang, Y., et al., *Graphene: a versatile nanoplatform for biomedical applications.* Nanoscale, 2012. **4**(13): p. 3833-3842.
4. Wang, J., et al., *Electrostatic Assembly of Peptide Nanofiber–Biomimetic Silver Nanowires onto Graphene for Electrochemical Sensors.* ACS Macro Letters, 2014. **3**(6): p. 529-533.
5. Promphet, N., et al., *An electrochemical sensor based on graphene/polyaniline/polystyrene nanoporous fibers modified electrode for simultaneous determination of lead and cadmium.* Sensors and Actuators B: Chemical, 2015. **207, Part A**(0): p. 526-534.
6. Wu, S., et al., *Graphene-Based Electrochemical Sensors.* Small, 2013. **9**(8): p. 1160-1172.
7. Kim, S., et al., *Highly Stable and Tunable n-Type Graphene Field-Effect Transistors with Poly(vinyl alcohol) Films.* ACS Applied Materials & Interfaces, 2015. **7**(18): p. 9702-9708.
8. Mosciatti, T., et al., *A Multifunctional Polymer-Graphene Thin-Film Transistor with Tunable Transport Regimes.* ACS Nano, 2015. **9**(3): p. 2357-2367.
9. Anagnostopoulos, G., et al., *Stress Transfer Mechanisms at the Submicron Level for Graphene/Polymer Systems.* ACS Applied Materials & Interfaces, 2015. **7**(7): p. 4216-4223.
10. Zeng, L., et al., *Graphene-supported platinum catalyst prepared with ionomer as surfactant for anion exchange membrane fuel cells.* Journal of Power Sources, 2015. **275**(0): p. 506-515.
11. Panzavolta, S., et al., *Structural reinforcement and failure analysis in composite nanofibers of graphene oxide and gelatin.* Carbon, 2014. **78**(0): p. 566-577.
12. Huang, L., et al., *Multifunctional Graphene Sensors for Magnetic and Hydrogen Detection.* ACS Applied Materials & Interfaces, 2015. **7**(18): p. 9581-9588.

13. Shakir, I., *High Energy Density based Flexible Electrochemical Supercapacitors from Layer-by-Layer Assembled Multiwall Carbon Nanotubes and Graphene.* Electrochimica Acta, 2014. **129**(0): p. 396-400.
14. Zhou, X., et al., *3-Dimensional porous N-doped graphene foam as a non-precious catalyst for the oxygen reduction reaction.* Journal of Materials Chemistry A, 2015. **3**(7): p. 3343-3350.
15. Khanna, S.K. and H.T.T. Phan, *High Strain Rate Behavior of Graphene Reinforced Polyurethane Composites.* Journal of Engineering Materials and Technology, 2015. **137**(2): p. 021005-021005.
16. Zhang, Y., L. Zhang, and C. Zhou, *Review of Chemical Vapor Deposition of Graphene and Related Applications.* Accounts of Chemical Research, 2013. **46**(10): p. 2329-2339.
17. Parvez, K., et al., *Exfoliation of Graphite into Graphene in Aqueous Solutions of Inorganic Salts.* Journal of the American Chemical Society, 2014. **136**(16): p. 6083-6091.
18. Khan, U., et al., *Solvent-Exfoliated Graphene at Extremely High Concentration.* Langmuir, 2011. **27**(15): p. 9077-9082.
19. Hummers, W.S. and R.E. Offeman, *Preparation of Graphitic Oxide.* Journal of the American Chemical Society, 1958. **80**(6): p. 1339-1339.
20. Botas, C., et al., *Critical temperatures in the synthesis of graphene-like materials by thermal exfoliation–reduction of graphite oxide.* Carbon, 2013. **52**(0): p. 476-485.
21. Sahoo, S., et al., *Graphene/polypyrrole nanofiber nanocomposite as electrode material for electrochemical supercapacitor.* Polymer, 2013. **54**(3): p. 1033-1042.
22. Barzegar, F., et al., *Preparation and characterization of poly(vinyl alcohol)/graphene nanofibers synthesized by electrospinning.* Journal of Physics and Chemistry of Solids, 2015. **77**(0): p. 139-145.
23. Sawada, K., S. Sakai, and M. Taya, *Enhanced productivity of electrospun polyvinyl alcohol nanofibrous mats using aqueous N,N-dimethylformamide solution and their application to lipase-immobilizing membrane-shaped catalysts.* Journal of Bioscience and Bioengineering, 2012. **114**(2): p. 204-208.
24. Oriero, D.A., et al., *A potential enzyme-encapsulating, ultrafine fiber for phenol detection.* Reactive and Functional Polymers, 2011. **71**(8): p. 870-880.

25. Ramalingam, K.J., et al., *Electrical measurement of PVA/graphene nanofibers for transparent electrode applications.* Synthetic Metals, 2014. **191**(0): p. 113-119.
26. Liu, Y., X. Dong, and P. Chen, *Biological and chemical sensors based on graphene materials.* Chemical Society Reviews, 2012. **41**(6): p. 2283-2307.
27. Darrell, H.R. and C. Iksoo, *Nanometre diameter fibres of polymer, produced by electrospinning.* Nanotechnology, 1996. **7**(3): p. 216.
28. Thoppey, N.M., et al., *Effect of Solution Parameters on Spontaneous Jet Formation and Throughput in Edge Electrospinning from a Fluid-Filled Bowl.* Macromolecules, 2012. **45**(16): p. 6527-6537.
29. Xu, X., et al., *Fabrication of high strength PVA/SWCNT composite fibers by gel spinning.* Carbon, 2010. **48**(7): p. 1977-1984.
30. Ramazani, S. and M. Karimi, *Electrospinning of poly(ε-caprolactone) solutions containing graphene oxide: Effects of graphene oxide content and oxidation level.* Polymer Composites, 2014: p. n/a-n/a.
31. Stachewicz, U., et al., *Manufacture of Void-Free Electrospun Polymer Nanofiber Composites with Optimized Mechanical Properties.* ACS Applied Materials & Interfaces, 2012. **4**(5): p. 2577-2582.
32. Fujikura, K., et al., *Preparation of electrospun fiber mats using siloxane-containing vaterite and biodegradable polymer hybrids for bone regeneration.* Journal of Biomedical Materials Research Part B: Applied Biomaterials, 2013. **101**(8): p. 1350-1358.
33. Tan, Y., Y. Song, and Q. Zheng, *Hydrogen bonding-driven rheological modulation of chemically reduced graphene oxide/poly(vinyl alcohol) suspensions and its application in electrospinning.* Nanoscale, 2012. **4**(22): p. 6997-7005.
34. Haward, S.J., et al., *Shear and Extensional Rheology of Cellulose/Ionic Liquid Solutions.* Biomacromolecules, 2012. **13**(5): p. 1688-1699.
35. Kim, J.E. and H.S. Lee, *Oscillatory shear induced gelation of graphene–poly(vinyl alcohol) composite hydrogels and rheological premonitor of ultra-light aerogels.* Polymer, 2014. **55**(1): p. 287-294.
36. Moayeri, A. and A. Ajji, *Fabrication of polyaniline/poly(ethylene oxide)/non-covalently functionalized graphene nanofibers via electrospinning.* Synthetic Metals, 2015. **200**(0): p. 7-15.

37. Du, Q., D.R. Harding, and H. Yang, *Helical peanut-shaped poly(vinyl pyrrolidone) ribbons generated by electrospinning.* Polymer, 2013. **54**(25): p. 6752-6759.
38. Sujith, K., et al., *Fabrication of highly porous conducting PANI-C composite fiber mats via electrospinning.* Materials Letters, 2012. **67**(1): p. 376-378.
39. Shahi, M., et al., *Electrospun PVA–PANI and PVA–PANI– composite nanofibers.* Scientia Iranica, 2011. **18**(6): p. 1327-1331.
40. Liu, Y., et al., *High-flux microfiltration filters based on electrospun polyvinylalcohol nanofibrous membranes.* Polymer, 2013. **54**(2): p. 548-556.
41. Mansur, H.S., et al., *FTIR spectroscopy characterization of poly (vinyl alcohol) hydrogel with different hydrolysis degree and chemically crosslinked with glutaraldehyde.* Materials Science and Engineering: C, 2008. **28**(4): p. 539-548.
42. Wang, F., et al., *Polyaniline microrods synthesized by a polyoxometalates/poly(vinyl alcohol) microfibers template.* Materials Letters, 2005. **59**(29–30): p. 3982-3985.
43. Shin, M.K., et al., *Enhanced conductivity of aligned PANI/PEO/MWNT nanofibers by electrospinning.* Sensors and Actuators B: Chemical, 2008. **134**(1): p. 122-126.